Redox Biology 41 (2021) 101947

Contents lists available at ScienceDirect

Redox Biology

journal homepage: www.elsevier.com/locate/redox

NOX4 promotes ferroptosis of astrocytes by oxidative stress-induced lipid peroxidation via the impairment of mitochondrial metabolism in Alzheimer's diseases

Min Woo Park [a], Hyeon Woo Cha [a], Junhyung Kim [a], Jung Han Kim [a], Haesung Yang [b,d], Sunmi Yoon [b,d], Napissara Boonpraman [b,d], Sun Shin Yi [b,d], Ik Dong Yoo [c,**], Jong-Seok Moon [a,*]

[a] Department of Integrated Biomedical Science, Soonchunhyang Institute of Medi-bio Science (SIMS), Soonchunhyang University, Cheonan, 31151, Chungcheongnam-do, Republic of Korea
[b] Department of Biomedical Laboratory Science, College of Medical Sciences, Soonchunhyang University, Asan, 31538, Chungcheongnam-do, Republic of Korea
[c] Department of Nuclear Medicine, Soonchunhyang University Hospital Cheonan, Cheonan, 31151, Chungcheongnam-do, Republic of Korea
[d] BK21 Four Project, Department of Biomedical Laboratory Science, General Graduate School, College of Medical Sciences, Soonchunhyang University, Asan, 31538, Chungcheongnam-do, Republic of Korea

ARTICLE INFO

Keywords:
NOX4
Ferroptosis
Mitochondrial metabolism
Oxidative stress
Alzheimer's disease

ABSTRACT

Oxidative stress has been implicated in the pathogenesis of Alzheimer's disease (AD). Mitochondrial dysfunction is linked to oxidative stress and reactive oxygen species (ROS) in neurotoxicity during AD. Impaired mitochondrial metabolism has been associated with mitochondrial dysfunction in brain damage of AD. While the role of NADPH oxidase 4 (NOX4), a major source of ROS, has been identified in brain damage, the mechanism by which NOX4 regulates ferroptosis of astrocytes in AD remains unclear. Here, we show that the protein levels of NOX4 were significantly elevated in impaired astrocytes of cerebral cortex from patients with AD and APP/PS1 double-transgenic mouse model of AD. The levels of 4-hydroxynonenal (4-HNE) and malondialdehyde (MDA), a marker of oxidative stress-induced lipid peroxidation, were significantly also elevated in impaired astrocytes of patients with AD and mouse AD. We demonstrate that the over-expression of NOX4 significantly increases the impairment of mitochondrial metabolism by inhibition of mitochondrial respiration and ATP production via the reduction of five protein complexes in the mitochondrial ETC in human astrocytes. Moreover, the elevation of NOX4 induces oxidative stress by mitochondrial ROS (mtROS) production, mitochondrial fragmentation, and inhibition of cellular antioxidant process in human astrocytes. Furthermore, the elevation of NOX4 increased ferroptosis-dependent cytotoxicity by the activation of oxidative stress-induced lipid peroxidation in human astrocytes. These results suggest that NOX4 promotes ferroptosis of astrocytes by oxidative stress-induced lipid peroxidation via the impairment of mitochondrial metabolism in AD.

1. Introduction

Alzheimer's disease (AD) is a progressive neurodegenerative disease and the most common cause of dementia characterized by impairment of memory and cognitive function [1]. Recent studies suggest that oxidative stress is a critical factor that contributes to the initiation and progression of AD [2–4]. Mitochondrial dysfunction plays an important role in the pathogenesis of AD as an early feature of AD [5,6]. Oxidative stress from mitochondrial dysfunction occurs in the early stage of AD [7,8]. Oxidative stress is characterized by the over-production of reactive oxygen species (ROS), damage of the mitochondrial respiratory chain, and imbalance of Ca^{2+} homeostasis [9,10]. Recent studies have shown the impairment of mitochondrial metabolism by multiple mitochondrial alterations in major neurodegenerative diseases such as AD and Parkinson's disease (PD) [11–13].

Astrocytes are the most numerous subtypes of glial cell population in the central nervous system (CNS) [14,15]. The roles of astrocytes have been linked to brain development and function such as synapse formation and function, control of neurotransmitters release and uptake, production of trophic factors and control of neuronal survival [16–20].

* Corresponding author.
** Corresponding author.
E-mail addresses: 92132@schmc.ac.kr (I.D. Yoo), jongseok81@sch.ac.kr (J.-S. Moon).

https://doi.org/10.1016/j.redox.2021.101947
Received 3 February 2021; Received in revised form 10 March 2021; Accepted 12 March 2021
Available online 19 March 2021

Astrocytes also play a key role in several homeostatic and neuroprotective functions and are essential for the integrity of the blood–brain barrier (BBB) [18]. Loss of supportive function by impaired astrocytes has been implicated in neurodegenerative diseases via neuronal death [21,22]. Previously, we have shown that the impairment of astrocytes is elevated in brains of patients with AD [23].

Mitochondrial metabolism is important for energy production and survival of brain cells in brain [24,25]. Mitochondrial metabolism in astrocytes plays a role in brain bioenergetics, neurotransmission and redox balance [24,25]. In physiological or pathological conditions, mitochondrial metabolism is critical for the regulation of redox in astrocytes [26–28]. In mitochondrial metabolic pathway, mitochondrial respiration and electron transport chain (ETC) play a critical role in ATP production through oxidative phosphorylation. The mitochondrial ETC consists of five protein complexes, including Complex I (NADH:ubiquinone oxidoreductase), Complex II (succinate dehydrogenase), Complex III (coenzyme Q:cytochrome *c* reductase), Complex IV (cytochrome *c* oxidase) and Complex V (ATP synthase), which are integrated into the inner mitochondrial membrane [29,30]. The impairment of mitochondrial ETC activity in mitochondrial metabolism leads to an increase of reactive oxygen species (ROS) production which occurs mainly at Complex I and Complex III [31].

Ferroptosis is a type of programmed cell death that is dependent on iron and the accumulation of lipid peroxides, mainly lipid hydroperoxides, which cause damage to the lipid bilayer of the plasma membrane through accelerated oxidation of membrane lipids [32,33]. The excessive production of ROS and the activation of lipid peroxidation are linked to ferroptosis-dependent cell death [32,33]. Mitochondrial damage has been found to be involved in lipid peroxidation and imbalance of iron homeostasis in neurodegenerative diseases such as AD and PD [34].

NADPH oxidases (NOXs) are a family of enzymes that produce ROS [35]. In most mammals, there are seven NOX isoforms (NOX1, NOX2, NOX3, NOX4, NOX5, dual oxidase (DUOX)1, and DUOX2) [35]. They are multi-subunit membrane-bound enzymes that catalyze the reduction of oxygen into superoxide by using NADPH as an electron donor and oxygen as an electron acceptor [35]. Among NOX isoforms, NOX4 is a major isoform in astrocytes [36]. NOX4 produces ROS constitutively [37]. However, the mechanisms by which NOX4 regulates ferroptosis of astrocytes by oxidative stress via impairment of mitochondrial metabolism in AD remains unclear.

Here, our results showed that the levels of NOX4 were significantly elevated in impaired astrocytes in patients with AD and APP/PS1 double-transgenic mouse model of AD. The levels of 4-HNE and MDA were also significantly elevated in impaired astrocytes of patients with AD and mouse AD. We found that the elevation of NOX4 promotes the impairment of mitochondrial metabolism by inhibition of mitochondrial respiration and ATP production in human astrocytes. The elevation of NOX4 induced mtROS production and mitochondrial fragmentation in human astrocytes. Notably, the elevation of NOX4 induced ferroptosis-dependent cytotoxicity by the activation of lipid peroxidation in human astrocytes. Our results suggest that NOX4 promotes ferroptosis of astrocytes by lipid peroxidation via the impairment of mitochondrial metabolism in AD.

2. Materials and methods

2.1. Human subjects study

Human subjects study was conducted in accordance with the Helsinki Declaration. The protocol was approved by the Institutional Review Board of Soonchunhyang University Hospital Cheonan (SCHCA 2020-03-030-001). A total of 12 paraffin embedded brain tissues including frontal cortex, occipital cortex, temporal cortex and parietal cortex from three donors with Alzheimer's diseases were obtained from The Netherlands Brain Bank. A total of four paraffin embedded adult normal brain tissues from four donors including frontal cortex (NBP2-77761), occipital cortex (NBP2-77766), temporal cortex (NBP2-77774) and parietal cortex (NBP2-77769) were obtained from Novus Biologicals (Minneapolis, MN, USA). For immunofluorescence analysis, brain tissues including temporal cortex and occipital cortex from patients with AD (AD) and non-AD (normal) were analyzed.

2.2. APP/PS1 mouse models of Alzheimer's disease

APP/PS1 double-transgenic mice (Stock no. 34829-JAX, B6; C3-Tg (APPswe, PSEN1dE9) 85Dbo/Mmjax) were obtained from the Jackson Laboratory (Bar Harbor, ME USA). APP/PS1 double-transgenic mouse models of Alzheimer's disease (AD) that overexpress mutated forms of the genes for human amyloid precursor protein (APP) and presenilin 1 (PS1).

2.3. Reagents and antibodies

The following antibodies were used: polyclonal rabbit anti-NOX4 (ab3517, Abcam, Cambridge, UK), polyclonal rabbit anti-4-HNE antibody (ab3517, Abcam, Cambridge, UK), polyclonal rabbit anti-Malondialdehyde (MDA) antibody (ab27642, Abcam, Cambridge, UK), monoclonal mouse anti-OXPHOS complex antibody (ab110413, Abcam, Cambridge, UK), monoclonal mouse anti-GFAP (#3670, Cell signaling technology, Danvers, MA, USA), polyclonal rabbit anti-Tomm20 antibody (sc-17764, Santa Cruz Biotechnology, Dallas, TX, USA), polyclonal rabbit anti-NRF2 antibody (#12721, Cell signaling technology, Danvers, MA, USA), polyclonal rabbit Histone H3 antibody (#9715, Cell signaling technology, Danvers, MA, USA) and monoclonal mouse anti-β-actin (A5316, Sigma-Aldrich, St. Louis, MO, USA). Fluoroshield™ with DAPI (F6057, Sigma-Aldrich, St. Louis, MO, USA) was used for nuclear staining and mounting. Sections were mounted onto gelatin-coated slides with Canada Balsam (Wako, Tokyo, Japan) following dehydration.

2.4. Human astrocytes

Human astrocytes were obtained from N7805100 (Thermo Fisher Scientific, Waltham, MA, USA) and #1800 (ScienCell Research Laboratories, Carlsbad, CA, USA). Human astrocytes are normal human cells derived from human brain tissue. Human astrocytes were cultured in Gibco™ Astrocyte Medium containing N-2 Supplement, Dulbecco's Modified Eagle Medium (DMEM), 10% (vol/vol) One Shot™ Fetal Bovine Serum (FBS), 100 units/ml penicillin and 100 mg/ml streptomycin (A1261301, Thermo Fisher Scientific, Waltham, MA, USA). For overexpression of human NOX4, Human astrocytes were seeded and transduced with pCMV6-AC-GFP constructs against human NOX4 (NM_016931) (RG208007, Origene, Rockville, MD, USA) or pCMV6-AC-GFP vector (PS100010, Origene).

2.5. Immunofluorescence analysis

For immunofluorescence analysis, brain tissues were sectioned from paraffin embedded tissue blocks at a thickness of 4 μm. Sections were permeabilized in 0.5% Triton-X (T8787, Sigma-Aldrich, St Louis, MO, USA), blocked in CAS-Block™ Histochemical Reagent (008120, Thermo Fisher Scientific, Waltham, MA, USA), and then stained with the following antibodies: polyclonal rabbit anti-NOX4 (1:100) (ab3517, Abcam, Cambridge, UK), polyclonal rabbit anti-4-HNE antibody (1:100) (ab46545, Abcam, Cambridge, UK), polyclonal rabbit anti-Tomm20 antibody (1:100) (sc-17764, Santa Cruz Biotechnology, Dallas, TX, USA), monoclonal mouse anti-GFAP (1:100) (#3670, Cell Signaling Technology, Danvers, MA, USA). Sections were then incubated with goat anti-rabbit IgG (H + L) Alexa Fluor 488 (1:100) (A11008, Thermo Fisher Scientific, Waltham, MA, USA), and goat anti-mouse IgG H&L Texas Red (1:100) (ab6787, Abcam, Cambridge, UK) secondary

antibody at 25 °C for 2 h. Fluoroshield™ with DAPI (F6057, Sigma-Aldrich, St. Louis, MO, USA) was used for nuclear staining. Stained brain sections were analyzed by THUNDER Imager Tissue (Leica Microsystems Ltd., Wetzlar, Germany). Stained brain sections were quantified by LAS X image-processing software (Leica Microsystems Ltd., Wetzlar, Germany) and ImageJ software v1.52a (Bethesda, MD, USA). To ensure objectivity, all measurements were performed with blinded conditions by two observers per experiment under identical conditions. Cells were plated and treated on autoclaved glass coverslips placed in 6-well cell culture plates. Cells were fixed in 4% paraformaldehyde (PFA), permeabilized in 0.5% Triton-X (T8787, Sigma-Aldrich, St. Louis, MO, USA), blocked in CAS-Block™ Histochemical Reagent (008120, Thermo Fisher Scientific, Waltham, MA, USA), and then stained as described above.

2.6. Mitochondrial respiration activity assay

For the mitochondrial function assay, human astrocytes (5×10^4 cells/well) were plated on XF96 cell culture microplates (101085-004, Agilent Technologies, Inc., Santa Clara, CA, USA). The oxygen consumption rate (OCR), a parameter of mitochondrial oxygen consumption and respiration, was measured by a Seahorse XF96e bioanalyzer using the XF Mito Stress Test Kit (103015-100, Agilent Technologies, Inc., Santa Clara, CA, USA) according to the manufacturer's instructions. The OCR levels were monitored and measured in cells treated with oligomycin (2 μM), FCCP (5 μM), rotenone (10 μM) and antimycin (10 μM).

2.7. Mitochondrial ATP production rate assay

For the mitochondrial ATP production assay, human astrocytes (5×10^4 cells/well) were plated on XF96 cell culture microplates (101085-004, Agilent Technologies, Inc., Santa Clara, CA, USA). Real-Time ATP production rate was measured by a Seahorse XF96e bioanalyzer using the XF Real-Time ATP Rate Assay Kit (103592-100, Agilent Technologies, Inc., Santa Clara, CA, USA) according to the manufacturer's instructions. The OCR levels were monitored and measured in cells that were treated with oligomycin (2 μM), rotenone (10 μM) and antimycin (10 μM).

2.8. Analysis of fragmented mitochondria by mitochondrial morphology

Fragmented mitochondria were determined by shortened, punctate, and rounded shape by mitochondria morphological analysis. Normal mitochondria were determined by filamentous shape and thread-like tubular structure. Consistent with earlier studies, the mitochondria within one cell were often either filamentous or fragmented. The cells which have the majority (>70%) of fragmented mitochondria were determined as the cells with mitochondrial fragmentation.

2.9. 3D images

Human astrocytes (2×10^4 cells) were seeded in FluoroDish TM (FD35-100, World Precision Instruments, Sarasota, FL, USA). Cells were transduced with pCMV6-AC-GFP constructs against human NOX4 (NM_016931) (RG208007, Origene, Rockville, MD, USA) or pCMV6-AC-GFP vector (PS100010, Origene). Cells were incubated for 24 h or 48 h 3D images were analyzed with 3D Cell Explorer (NANOLIVE, Ecublens, Switzerland). Images were representative images from a total of 100 cells in ten individual images per group.

2.10. Immunoblot analysis

Cells were harvested and lysed in NP40 Cell Lysis Buffer (FNN0021, Thermo Fisher Scientific, Waltham, MA, USA). Lysates were centrifuged at 15,300×*g* for 10 min at 4 °C, and the supernatants were obtained. The protein concentrations of the supernatants were determined by using the Bradford assay kit (500-0006, Bio-Rad Laboratories, Hercules, CA, USA). Proteins were electrophoresed on NuPAGE 4%–12% Bis-Tris gels (Thermo Fisher Scientific, Waltham, MA, USA) and transferred to Protran nitrocellulose membranes (10600001, GE Healthcare Life science, Pittsburgh, PA, USA). Membranes were blocked in 5% (w/v) bovine serum albumin (BSA) (9048-46-8, Santa Cruz Biotechnology, Dallas, TX, USA) in TBS-T (TBS (170-6435, Bio-Rad Laboratories, Hercules, CA, USA)) and 1% (v/v) Tween-20 (170-6531, Bio-Rad Laboratories)) for 30 min at 25 °C. Membranes were incubated with primary antibody (1:1000) diluted in 1% (w/v) BSA in TBS-T for 16 h at 4 °C and then with the horseradish peroxidase (HRP)-conjugated secondary antibody (goat anti–rabbit IgG–HRP (sc-2004) (1:2500) and goat anti–mouse IgG–HRP (sc-2005) (1:2500) from Santa Cruz Biotechnology, Dallas, TX, USA) diluted in TBS-T for 0.5 h at room temperature. Immunoreactive bands were detected with a SuperSignal West Pico Chemiluminescent Substrate (34078, Thermo Scientific, Waltham, MA, USA).

2.11. Mitochondrial ROS (mtROS) production analysis

Mitochondrial ROS levels were measured by MitoSOX (M36008, Invitrogen) staining. Cells (2×10^4 cells) were plated in 6-well cell culture plates. Cells were transduced with pCMV6-AC-GFP constructs against human NOX4 (NM_016931) (RG208007, Origene, Rockville, MD, USA)) or pCMV6-AC-GFP vector (PS100010, Origene). Cells were then incubated for 24 h. Cells were washed with PBS, treated with trypsin and resuspended in OPTI-MEM (31985070, Invitrogen). Data were acquired with a NucleoCounter® NC-3000 (ChemoMetec Inc, Bohemia, NY, USA) and analyzed with FlowJo analytical software (TreeStar).

2.12. Measurement of GSH, ratio of GSH/GSSG and GSSG

Glutathione (GSH) was measured from protein lysate of human astrocytes using Reduced Glutathione (GSH) Assay Kit (#K464-100, BioVision, Milpitas, CA, USA) following the manufacturer's instructions. The ratio of GSH/oxidized glutathione (GSSG) and GSSG were measured from protein lysate of human astrocytes using Glutathione Fluorometric Assay Kit (#K264-100, BioVision, Milpitas, CA, USA) following the manufacturer's instructions. The ratio of GSH/GSSG was determined by the ratio of GSH squared over GSSG and presented as $GSH^2/GSSG$.

2.13. Isolation of nuclear and cytosolic protein

The nuclear and cytosolic protein were isolated from human astrocytes using Nuclear/Cytosol Fractionation Kit (#K266-25, BioVision, Milpitas, CA, USA) following the manufacturer's instructions.

2.14. Measurement of HO-1 levels and activity

The levels of HO-1 were measured from human astrocytes using Heme Oxygenase 1 (HO1) (Human) ELISA Kit (#E4507-100, BioVision, Milpitas, CA, USA) following the manufacturer's instructions. The activity of HO-1 was analyzed by the quantification of bilirubin production in human astrocytes using Bilirubin (Total and Direct) Colorimetric Assay Kit (#K553-100, BioVision, Milpitas, CA, USA) following the manufacturer's instructions.

2.15. Measurement of GCLC levels and GCL activity

The levels of glutamate cysteine ligase catalytic subunit (GCLC) were measured from human astrocytes using Human GCLC ELISA Kit (ab233632, Abcam, Cambridge, UK) following the manufacturer's instructions. The activity of GCL was measured from human astrocytes using glutamate cysteine ligase, GCL Assay Kit (MBS779411, MyBioSource, Inc., San Diego, CA, USA) following the manufacturer's

instructions.

2.16. Measurement of iron accumulation

The accumulation of iron was measured from human astrocytes using Iron Colorimetric Assay Kit (#K390-100, BioVision, Milpitas, CA, USA) following the manufacturer's instructions.

2.17. Cell cytotoxicity assay

Cell cytotoxicity was measured from culture medium of human astrocytes using an LDH-Cytotoxicity Colorimetric Assay Kit II (#K313-500, BioVision, Milpitas, CA, USA) following the manufacturer's instructions. Human astrocytes (2×10^5 cells in 6-well cell culture plate) were seeded and transduced with pCMV6-AC-GFP constructs against human NOX4 (NM_016931) (RG208007, Origene, Rockville, MD, USA) or pCMV6-AC-GFP vector (PS100010, Origene). Cells were then incubated for 24 h.

2.18. Statistical analysis

The assumptions of normality and homogeneity of variance were assessed. A Shapiro-Wilk test was conducted for normal distribution. Levene's test was conducted for the homogeneity of variance. Data are random, independent, normally distributed, and have a common variance. All data are presented as mean ± standard deviation (SD) or standard error of the mean (SEM). All statistical analysis was performed using a two-tailed Student's t-test for comparison of two groups, and analysis of variance (ANOVA) (with post hoc comparisons using Dunnett's test) using a statistical software package (GraphPad Prism version 8.0, GraphPad Software Inc., San Diego, CA, USA) for comparison of multiple groups. P values (*, $p < 0.05$, **, $p < 0.01$, ***, $p < 0.001$) were considered statistically significant.

3. Results

3.1. The levels of NOX4 are elevated in impaired astrocytes of the cortex region from patients with Alzheimer's diseases

To investigate the role of NOX4 in the impairment of astrocytes in patients with AD, we analyzed whether the protein levels of NOX4 were elevated in astrocytes on cortex of brain from patients with AD (Table S1). We measured the protein levels of NOX4 in GFAP-positive astrocytes on temporal cortex tissues of brain from patients with AD or non-AD donor (Normal) using immunofluorescence staining (Fig. 1A and B). Immunofluorescence staining revealed that the intensity of NOX4-positive staining in GFAP-positive astrocytes was increased in molecular layer (ML) of the cortex region of patients with AD (AD) relative to non-AD donor (Normal) (Fig. 1A and Fig. S1). Moreover, the intensity of NOX4-positive staining was elevated in impaired GFAP-

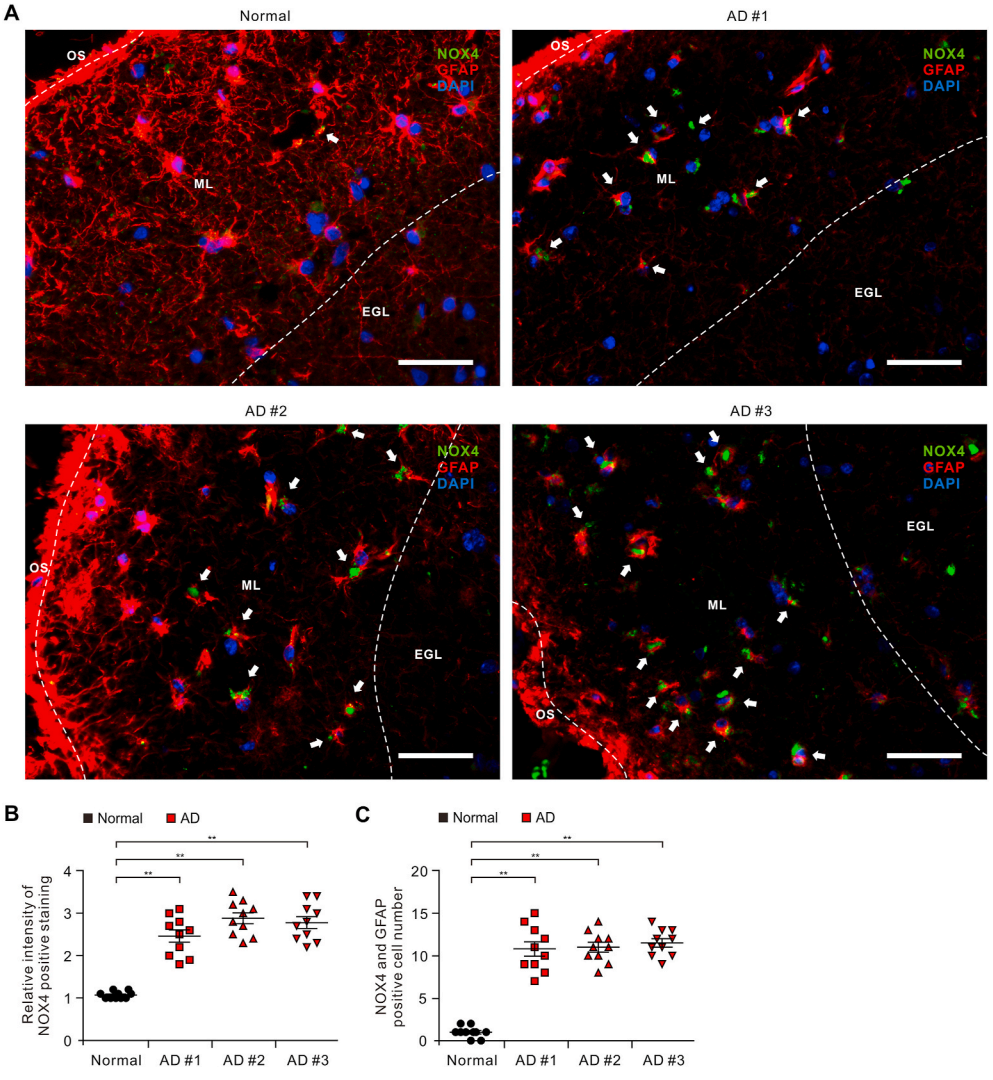

Fig. 1. The levels of NOX4 are elevated in impaired astrocytes of the cortex region from patients with Alzheimer's diseases. (A) Representative immunofluorescence images of NOX4 protein expression in cerebral cortex region from patients with AD (AD #1, AD #2, AD #3) or non-AD (normal) showing NOX4 (green) in astrocytes expressing astrocytes marker GFAP (red) around molecular layer (ML) (n = 3 per group, n = 10 images per individual subject). DAPI-stained nuclei are shown in blue. OS, Outer surface; ML, Molecular layer; EGL, External granular layer. Scale bars, 20 μm. White arrows indicate NOX4 and GFAP positive cells. Symbols, which are expressed by white dotted line, indicate the distinct area among OS, ML, and EGL. (B) Quantification of intensity for NOX4 positive staining in astrocytes from immunofluorescence images in the cerebral cortex region from patients with AD (AD #1, AD #2, AD #3) or non-AD (normal) (n = 3 per group, n = 10 images per individual subject). Data are mean ± standard deviation (SD). **, $p < 0.01$ by Student's two-tailed *t*-test. (C) Quantification of NOX4 positive astrocytes from immunofluorescence images in the cerebral cortex region from patients with AD (AD #1, AD #2, AD #3) or non-AD (normal) (n = 3 per group, n = 10 images per individual subject). Data are mean ± standard deviation (SD). **, $p < 0.01$ by Student's two-tailed *t*-test. (For interpretation of the references to colour in this figure legend, the reader is referred to the Web version of this article.)

positive astrocytes in ML of the cortex region of patients with AD (AD) compared to non-AD donor (Normal) (Fig. 1A and B). Furthermore, the length of GFAP-positive filaments was shortened and the shape of GFAP-positive filaments showed shrinkage in astrocytes of patients with AD (AD) compared to non-AD donor (Normal) (Fig. 1A). Notably, the number of impaired astrocytes which have the positive subcellular co-localization between NOX4 and GFAP was significantly increased in patients with AD (AD) (Fig. 1C). The levels of NOX4 were generally higher in every individual patient with AD relative to non-AD donor (Normal). These results suggest that the protein levels of NOX4 are elevated in impaired astrocytes of patients with AD.

3.2. The levels of oxidative stress-induced lipid peroxidation are elevated in impaired astrocytes of the cortex region from patients with Alzheimer's diseases

Since the protein levels of NOX4 were elevated in impaired astrocytes of patients with AD, we investigated the role of NOX4 in oxidative stress of impaired astrocytes of patients with AD. We analyzed whether the levels of oxidative stress-induced lipid peroxidation were elevated in impaired astrocytes on cortex of brains from patients with AD. We measured the protein levels of 4-hydroxynonenal (4-HNE), a marker of oxidative stress-induced lipid peroxidation and cytotoxicity, in GFAP-positive astrocytes on temporal cortex tissues of brain from patients with AD or non-AD donor (Normal) using immunofluorescence staining (Fig. 2A). Immunofluorescence staining revealed that the intensity of 4-HNE-positive staining in GFAP-positive astrocytes was increased in molecular layer (ML) of the cortex region of patients with AD (AD) relative to non-AD donor (Normal) (Fig. 2A and B and Fig. S2). Moreover, the intensity of 4-HNE-positive staining was elevated in impaired GFAP-positive astrocytes in ML of the cortex region of patients with AD (AD) compared to non-AD donor (Normal) (Fig. 2A and B). Notably, the number of impaired astrocytes which have the positive subcellular co-localization between 4-HNE and GFAP was significantly increased in patients with AD (AD) (Fig. 2C). Consistently, the intensity of malondialdehyde (MDA), a final product of lipid peroxidation during oxidative stress, positive staining in GFAP-positive astrocytes and the number of impaired astrocytes which have the positive subcellular co-localization between MDA and GFAP was increased in molecular layer (ML) of the cortex region of patients with AD (AD) relative to non-AD donor (Normal) (Fig. S3). The levels of 4-HNE and MDA were generally higher in every individual patient with AD. Moreover, the expression of 4-HNE was co-localized in NOX4-positive astrocytes of patients with AD (AD) relative to non-AD donor (Normal) (Fig. 2D and Fig. S4). The number of NOX4 and 4-HNE positive astrocytes was significantly increased in patients with AD (AD) relative to non-AD donor (Normal) (Fig. 2E). These results suggest that the levels of oxidative stress-induced lipid peroxidation are elevated in impaired astrocytes of patients with AD.

3.3. The levels of NOX4 are elevated in impaired astrocytes of the cortex region from brains of APP/PS1 mice

Next, we investigated the role of NOX4 in the impairment of astrocytes of APP/PS1 double-transgenic mouse model of AD. We analyzed whether the protein levels of NOX4 were elevated in impaired astrocytes on cortex of brain from APP/PS1 mice. We measured the protein levels of NOX4 in GFAP-positive astrocytes on cortex from APP/PS1 mice or wild-type (WT) mice using immunofluorescence staining (Fig. 3A and Fig. S5). Immunofluorescence staining revealed that the intensity of NOX4-positive staining in GFAP-positive astrocytes was increased in the cortex region of APP/PS1 mice compared to WT mice (Fig. 3A and B). Moreover, the number of impaired astrocytes which have the positive subcellular co-localization between NOX4 and GFAP was significantly increased in APP/PS1 mice than in WT mice (Fig. 3C). These results suggest that the protein levels of NOX4 are elevated in impaired astrocytes of APP/PS1 mice.

3.4. The levels of oxidative stress-induced lipid peroxidation are elevated in impaired astrocytes of the cortex region from brains of APP/PS1 mice

We investigated the role of NOX4-derived oxidative stress in impaired astrocytes of APP/PS1 mice. We analyzed whether the levels of oxidative stress-induced lipid peroxidation were elevated in impaired astrocytes on cortex of brain from APP/PS1 mice. We measured the protein levels of 4-HNE in GFAP-positive astrocytes on cortex of brain from APP/PS1 mice or wild-type (WT) mice using immunofluorescence staining (Fig. 4A). Immunofluorescence staining revealed that the intensity of 4-HNE-positive staining in GFAP-positive astrocytes was increased of the cortex region of APP/PS1 mice compared to WT mice (Fig. 4A and C and Fig. S6). Moreover, the intensity of 4-HNE-positive staining was elevated in impaired GFAP-positive astrocytes in the cortex region of APP/PS1 mice. Furthermore, the number of impaired astrocytes which have the positive subcellular co-localization between 4-HNE and GFAP was significantly increased in APP/PS1 mice relative to WT mice (Fig. 4D). Similar with these results, the intensity of MDA-positive staining in GFAP-positive astrocytes (Fig. 4B and E and Fig. S6) and the number of impaired astrocytes which have the positive subcellular co-localization between MDA and GFAP (Fig. 4F) was increased in the cortex region of APP/PS1 mice compared to WT mice. Moreover, the expression of 4-HNE was co-localized in NOX4-positive astrocytes of APP/PS1 mice compared to WT mice (Fig. 4G and Fig. S7). The number of NOX4 and 4-HNE positive astrocytes was significantly increased in APP/PS1 mice compared to WT mice (Fig. 4H). These results suggest that the levels of oxidative stress-induced lipid peroxidation are elevated in impaired astrocytes of APP/PS1 mice.

3.5. The elevation of NOX4 promotes oxidative stress by impairment of mitochondrial metabolism via inhibition of mitochondrial respiration and ATP production in human astrocytes

We investigated the underlying molecular mechanism by which the elevation of NOX4 induced oxidative stress in impaired astrocytes during AD. We examined whether NOX4 could promote oxidative stress via mitochondrial dysfunction in human astrocytes. We analyzed the effects of NOX4 elevation on the activity of mitochondrial metabolism such as mitochondrial respiration, electron transport chain (ETC) activity and ATP production. First, we measured the OCR as a parameter of mitochondrial respiration activity based on the quantification of oxygen consumption. The activity of mitochondrial respiration was measured by the sequential addition of oligomycin (a selective inhibitor for mitochondrial respiration), FCCP (a potent uncoupler of mitochondrial oxidative phosphorylation), rotenone and antimycin (specific inhibitors of mitochondrial complex I and complex III). The basal levels of OCR were significantly suppressed by NOX4 over-expression relative to control (Fig. 5A and B). Moreover, the levels of OCR in response to oligomycin and FCCP were significantly reduced by NOX4 over-expression compared to control (Fig. 5A and B). Next, we investigated the molecular target in the regulation of mitochondrial respiration pathway by NOX4 elevation in human astrocytes. We analyzed the levels of five protein complexes in the mitochondrial ETC including NADH: Ubiquinone Oxidoreductase Subunit B8 (NDUFB8) for Complex I, succinate dehydrogenase complex iron sulfur subunit B (SDHB) for Complex II, ubiquinol-cytochrome c reductase core protein 2 (UQCRC2) for Complex III, mitochondrially encoded cytochrome *c* oxidase I (MTCO1) for Complex IV and ATP synthase F1 subunit alpha (ATP5F1A) for Complex V, which are critical enzymes for mitochondrial respiration and oxidative phosphorylation, in human astrocytes (Fig. 5C and Fig. S8). Consistent with the levels of OCR, over-expression of NOX4 significantly suppressed the protein levels of five mitochondrial oxidative phosphorylation enzyme complexes compared to control. NOX4 over-expression significantly reduces the production of ATP relative to control (Fig. 5D). We examined whether impairment of mitochondrial metabolism by NOX4 elevation could induce oxidative stress in human

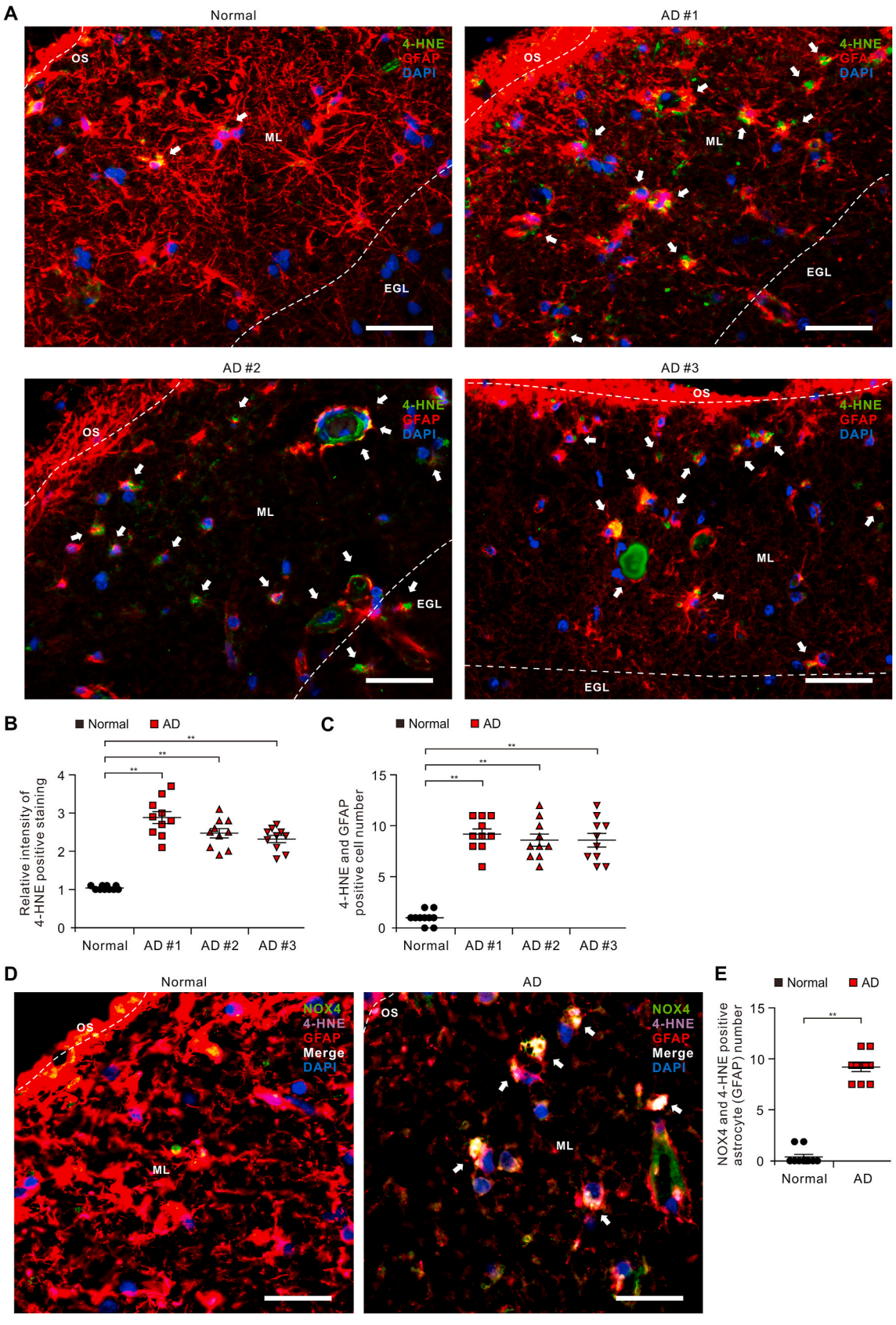

(caption on next page)

Fig. 2. The levels of oxidative stress-induced lipid peroxidation are elevated in impaired astrocytes of the cortex region from patients with Alzheimer's diseases.

(A) Representative immunofluorescence images of 4-HNE protein expression in cerebral cortex region from patients with AD (AD #1, AD #2, AD #3) or non-AD (normal) showing 4-HNE (green) in astrocytes expressing astrocytes marker GFAP (red) around molecular layer (ML) (n = 3 per group, n = 10 images per individual subject). DAPI-stained nuclei are shown in blue. OS, Outer surface; ML, Molecular layer; EGL, External granular layer. Scale bars, 20 μm. White arrows indicate 4-HNE and GFAP positive cells. Symbols, which are expressed by white dotted line, indicate the distinct area among OS, ML, and EGL. (B) Quantification of intensity of 4-HNE positive staining in astrocytes from immunofluorescence images in the cerebral cortex region from patients with AD (AD #1, AD #2, AD #3) or non-AD (normal) (n = 3 per group, n = 10 images per individual subject). Data are mean ± standard deviation (SD). **, $p < 0.01$ by Student's two-tailed *t*-test. (C) Quantification of 4-HNE positive astrocytes from immunofluorescence images in the cerebral cortex region from patients with AD (AD #1, AD #2, AD #3) or non-AD (normal) (n = 3 per group, n = 10 images per individual subject). Data are mean ± standard deviation (SD). **, $p < 0.01$ by Student's two-tailed *t*-test. (D) Representative immunofluorescence images of 4-HNE protein expression in NOX4-positive astrocytes of patients with AD (AD) or non-AD (normal) showing 4-HNE (purple) in NOX4 (green)-positive astrocytes expressing astrocytes marker GFAP (red) around molecular layer (ML) (n = 10 images per individual subject). DAPI-stained nuclei are shown in blue. Scale bars, 10 μm. White arrows indicate the co-localization of 4-HNE in NOX4-positive astrocytes. (E) Quantification of NOX4 and 4-HNE positive astrocytes from immunofluorescence images in the cerebral cortex region from patients with AD (AD) or non-AD (normal) (n = 10 images per individual subject). Data are mean ± standard deviation (SD). **, $p < 0.01$ by Student's two-tailed *t*-test. (For interpretation of the references to colour in this figure legend, the reader is referred to the Web version of this article.)

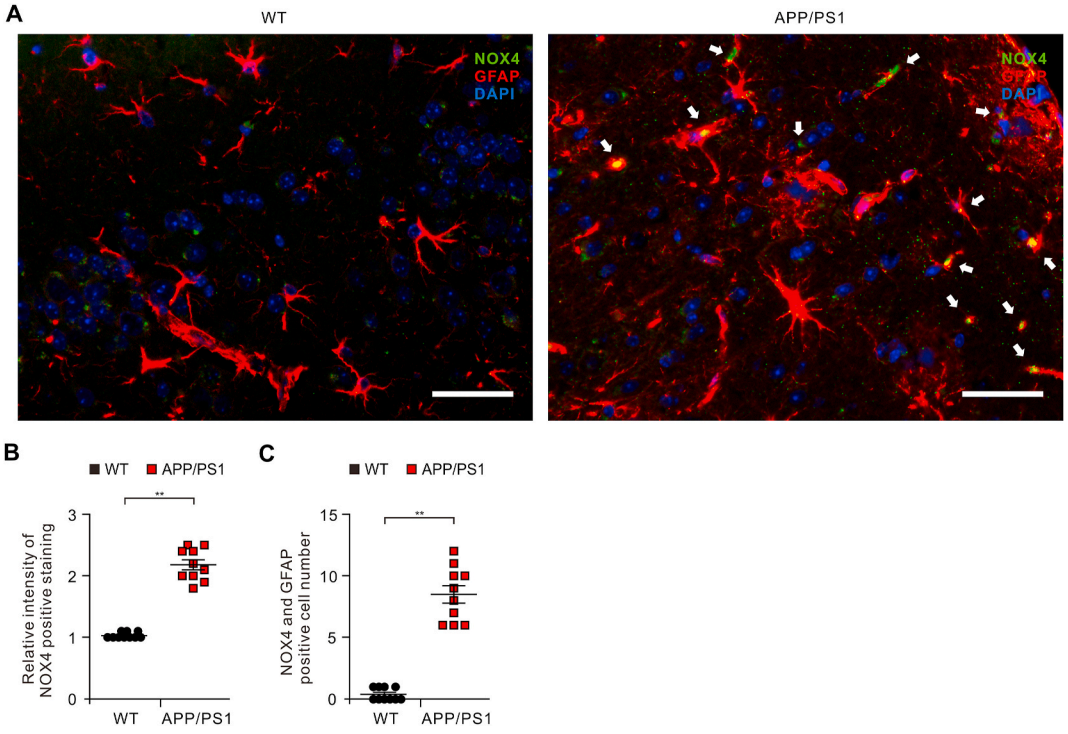

Fig. 3. The levels of NOX4 are elevated in impaired astrocytes of the cortex region from brain of APP/PS1 mice.

(A) Representative immunofluorescence images of NOX4 protein expression in cortex region from brain of APP/PS1 mice (APP/PS1) or wild-type mice (WT) showing NOX4 (green) in astrocytes expressing astrocytes marker GFAP (red) (n = 5 per group, n = 10 images per individual subject). DAPI-stained nuclei are shown in blue. Scale bars, 20 μm. White arrows indicate NOX4 and GFAP positive cells. (B) Quantification of intensity for NOX4 positive staining in astrocytes from immunofluorescence images in the cortex region from brains of APP/PS1 mice (APP/PS1) or wild-type mice (WT) (n = 5 per group, n = 10 images per individual subject). Data are mean ± standard deviation (SD). **, $p < 0.01$ by Student's two-tailed *t*-test. (C) Quantification of NOX4 positive astrocytes from immunofluorescence images in the cortex region from brains of APP/PS1 mice (APP/PS1) or wild-type mice (WT) (n = 5 per group, n = 10 images per individual subject). Data are mean ± standard deviation (SD). **, $p < 0.01$ by Student's two-tailed *t*-test. (For interpretation of the references to colour in this figure legend, the reader is referred to the Web version of this article.)

astrocytes. We analyzed the levels of mitochondrial ROS (mtROS) production and the morphological impairment of mitochondria by NOX4 over-expression in human astrocytes. Over-expression of NOX4 significantly increased the production of mtROS compared to control (Fig. 5E). We next analyzed morphological impairment of mitochondria caused by NOX4 over-expression through immunofluorescence staining with Tomm20, an outer mitochondrial membrane protein (Fig. 5F and G). Immunofluorescence staining revealed that elevation of NOX4 induced the fragmentation of mitochondria compared to control (Fig. 5F). The number of cells showing the fragmentation of mitochondria was significantly increased by NOX4 over-expression relative to control (Fig. 5G). These results suggest that the elevation of NOX4 promotes oxidative stress by impairment of mitochondrial metabolism via inhibition of mitochondrial respiration and ATP production in human astrocytes.

3.6. NOX4-induced mitochondrial metabolic impairment induces oxidative stress by inhibition of cellular antioxidant process in human astrocytes

Next, we investigated whether the NOX4-induced mitochondrial metabolic impairment could induce oxidative stress by inhibition of cellular antioxidant process in human astrocytes. We analyzed the status of glutathione (GSH) and ratio of reduced GSH to oxidized glutathione

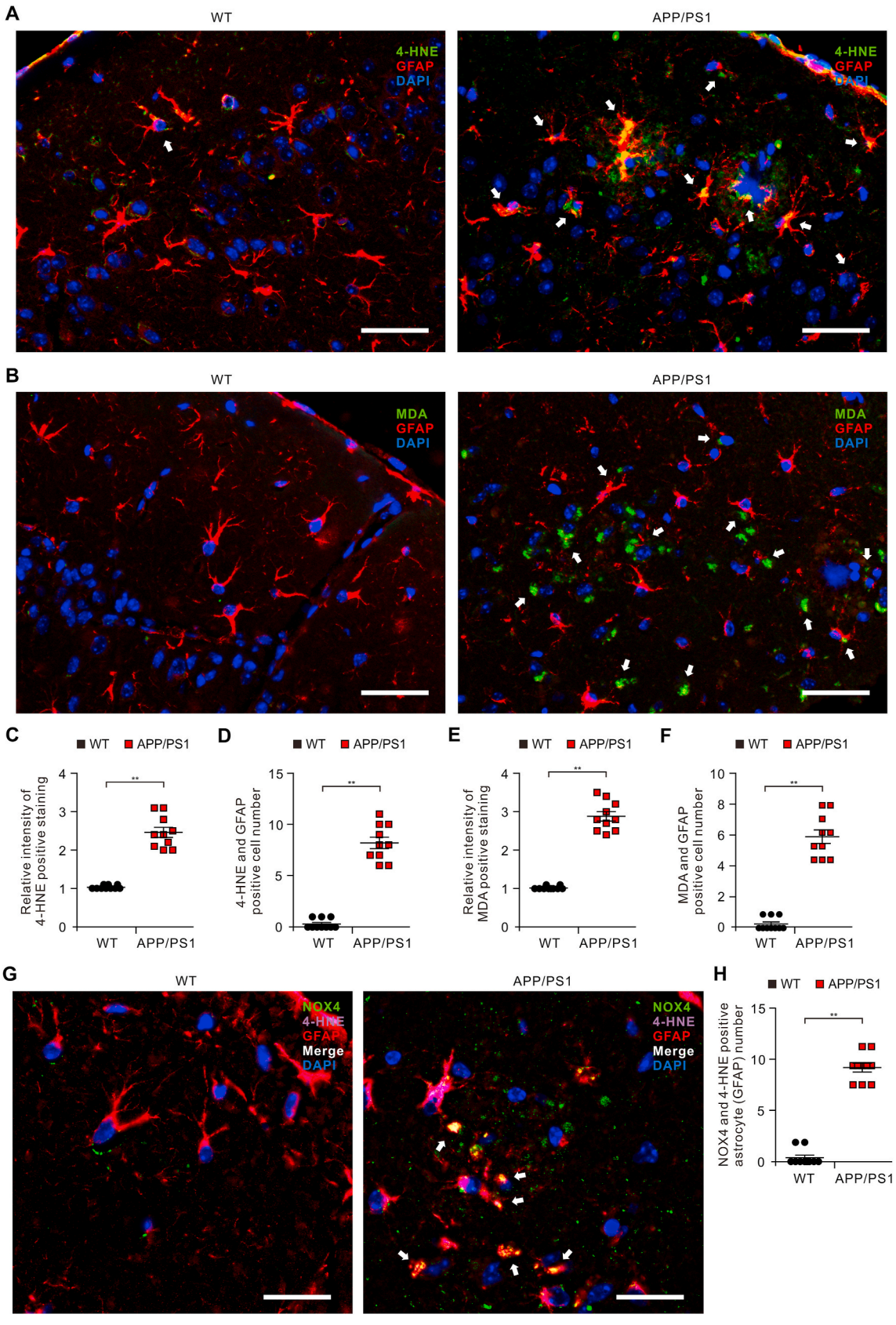

(caption on next page)

Fig. 4. The levels of oxidative stress-induced lipid peroxidation are elevated in impaired astrocytes of the cortex region from brains of APP/PS1 mice. (A) Representative immunofluorescence images of 4-HNE protein expression in cortex region from brain of APP/PS1 mice (APP/PS1) or wild-type mice (WT) showing 4-HNE (green) in astrocytes expressing astrocytes marker GFAP (red) (n = 5 per group, n = 10 images per individual subject). DAPI-stained nuclei are shown in blue. Scale bars, 20 μm. White arrows indicate 4-HNE and GFAP positive cells. (B) Quantification of 4-HNE positive staining in astrocytes from immunofluorescence images in the cortex region from brains of APP/PS1 mice (APP/PS1) or wild-type mice (WT) (n = 5 per group, n = 10 images per individual subject). Data are mean ± standard deviation (SD). **, $p < 0.01$ by Student's two-tailed *t*-test. (C) Quantification of 4-HNE positive astrocytes from immunofluorescence images of the cortex region from brains of APP/PS1 mice (APP/PS1) or wild-type mice (WT) (n = 5 per group, n = 10 images per individual subject). Data are mean ± standard deviation (SD). **, $p < 0.01$ by Student's two-tailed *t*-test. (D) Representative immunofluorescence images of 4-HNE protein expression in NOX4-positive astrocytes of APP/PS1 mice (APP/PS1) or wild-type mice (WT) showing 4-HNE (purple) in NOX4 (green)-positive astrocytes expressing astrocytes marker GFAP (red) (n = 10 images per individual subject). DAPI-stained nuclei are shown in blue. Scale bars, 10 μm. White arrows indicate the co-localization of 4-HNE in NOX4-positive astrocytes. (E) Quantification of NOX4 and 4-HNE positive astrocytes from immunofluorescence images in the cortex region from APP/PS1 mice (APP/PS1) or wild-type mice (WT) (n = 10 images per individual subject). Data are mean ± standard deviation (SD). **, $p < 0.01$ by Student's two-tailed *t*-test. (For interpretation of the references to colour in this figure legend, the reader is referred to the Web version of this article.)

(GSSG) as an indicator of oxidative stress. The elevation of NOX4 significantly reduced the levels of glutathione (GSH) and the ratio of GSH/oxidized glutathione (GSSG) relative to control (Fig. 6A and B). Also, the elevation of NOX4 increased the levels of GSSG compared to control (Fig. 6C). Since NOX4 leads to reduced GSH and the ratio GSH/GSSG, we next examined whether NOX4 could affect the nuclear factor erythroid 2–related factor 2 (NRF2) signaling pathway, a key regulator of the cellular antioxidant response, in human astrocytes. The elevation of NOX4 inhibited the nuclear translocation of NRF2 from cytosol compared to control (Fig. 6D and Fig. S9). Moreover, the levels and activity of heme oxygenase-1 (HO-1) (Fig. 6E and F) and glutamate cysteine ligase (GCL) (Fig. 6E and F) as target genes of NRF2 were significantly suppressed by NOX4 over-expression in human astrocytes. These results suggest that NOX4-induced mitochondrial metabolic impairment induces oxidative stress by inhibition of cellular antioxidant process in human astrocytes.

3.7. NOX4 promotes ferroptosis by oxidative stress-induced lipid peroxidation in human astrocytes

To investigate the molecular mechanism by which NOX4 regulates oxidative stress-induced cell death of astrocytes in AD, we examined whether elevation of NOX4 could promote ferroptosis by oxidative stress-induced lipid peroxidation in human astrocytes. Since the levels of 4-HNE, a marker for ferroptosis, were elevated in impaired astrocytes of patients with AD, we analyzed the changes of oxidative stress-induced lipid peroxidation and morphological impairment by NOX4 over-expression in human astrocytes. We measured the protein levels of 4-HNE in human astrocytes using immunofluorescence staining. Notably, immunofluorescence staining revealed that the elevation of NOX4 increased the levels of 4-HNE protein compared to control (Fig. 7A). The shape of cells showed shrinkage and lipid peroxidation-derived droplet in the plasma membrane was increased by NOX4 over-expression relative to control (Fig. 7A). The number of 4-HNE-positive cells was significantly increased by NOX4 over-expression relative to control (Fig. 7B). Moreover, the levels of 4-HNE were increased by NOX4 over-expression compared to control (Fig. 7C and S10). Moreover, the elevation of NOX4 increased the levels of MDA relative to control (Fig. 7C and Fig. S10). Notably, the elevation of NOX4 increased the accumulation of iron, a specific marker of ferroptosis, compared to control (Fig. 7D). Next, we analyzed the morphological changes of cytotoxicity after elevation of NOX4 in human astrocytes using 3D analyzer (Fig. 7E). Consistent with the levels of 4-HNE, the elevation of NOX4 induced the morphological features of cytotoxicity including shrinkage of cytosolic area and blebbing relative to control (Fig. 7E). Moreover, the number of morphological dead cells by NOX4 elevation was significantly increased compared to control (Fig. 7F). Consistent with results of morphological analysis, the elevation of NOX4 significantly increased the levels of cytotoxicity relative to control (Fig. 7G). These results suggest that NOX4 promotes ferroptosis by oxidative stress-induced lipid peroxidation in human astrocytes.

In summary, our results demonstrate that elevated NOX4 promotes ferroptosis by oxidative stress-induced lipid peroxidation via impairment of mitochondrial function in Alzheimer's diseases (Fig. 8).

4. Discussion

Here we demonstrate that NOX4 promotes ferroptosis of astrocytes in AD. We suggest that the elevation of NOX4 induces the impairment of mitochondrial metabolism and oxidative stress-induced lipid peroxidation in human astrocytes. Our findings provide a molecular mechanism by which the elevation of NOX4 is critical for ferroptosis of astrocytes by oxidative stress-induced lipid peroxidation via the impairment of mitochondrial metabolism in the pathogenesis of AD.

Mitochondrial dysfunction has been associated with the pathogenesis of AD [5,6]. The suppression of mitochondria-related oxygen metabolism has been identified in the frontal, parietal and temporal cortex in brains of patients with AD [38–40]. The levels of cerebral blood (CBF) and cerebral metabolic rate for oxygen ($CMRO_2$) in the medial temporal region were decreased in patient with AD [38]. Also, the expression of genes and proteins encoding subunits of the mitochondrial electron transport chain (ETC) in mitochondrial metabolic pathways was reduced in brain tissues of patients with AD [41]. However, the underlying molecular mechanism which by impairment of mitochondrial metabolic activity and oxidative stress in astrocytes of AD is not fully understood yet. Our results suggest that NOX4 could be an upstream molecular target in the impairment of mitochondrial oxygen metabolism by inhibition of mitochondrial respiration and ATP production in astrocytes during AD. Our results showed that the elevation of NOX4 suppresses the mitochondrial respiration and ATP production rate via the reduction of five protein complexes in the mitochondrial ETC of human astrocytes.

NOX4 is linked to oxidative stress and ROS production in brain injury [42,43]. Oxidative stress is linked to amyloid-beta (Aβ) toxicity in AD [44,45]. Astrocytes are associated with oxidative stress by Aβ-induced ROS production [46]. In APP/PS1 mouse model of AD, the elevation of NOX activity is linked to cognitive impairment [47]. Consistent with previous study [46], our results showed that the elevation of NOX4 promoted excessive mtROS production in human astrocytes. Our findings suggest that NOX4 might be critical for oxidative stress by ROS production in astrocytes during AD. Since NOX4 is a constitutively active form among the NOX isoforms, the activity of NOX4 depends on its expression [37]. In our results, the elevation of NOX4 protein levels in astrocytes of brains from patients with AD and APP/PS1 mice may represent a high activity of NOX4 in AD. Similarly, a recent study has suggested that NOX4 in pericytes is the major source of ROS which is involved in the constriction of capillaries early in the response to Aβ [48]. Regarding the form of astrocytes, reactive astrocytes are an activated form of astrocytes in response to toxic materials [49]. The role of reactive astrocytes remains unclear in terms of plaque formation, Aβ clearance and plaque growth restriction [50,51]. Although we found impaired astrocytes, which have the high levels of NOX4, in cortex of patients with AD, it was unclear whether these impaired astrocytes have a function of reactive astrocytes in AD. Further study for the role of

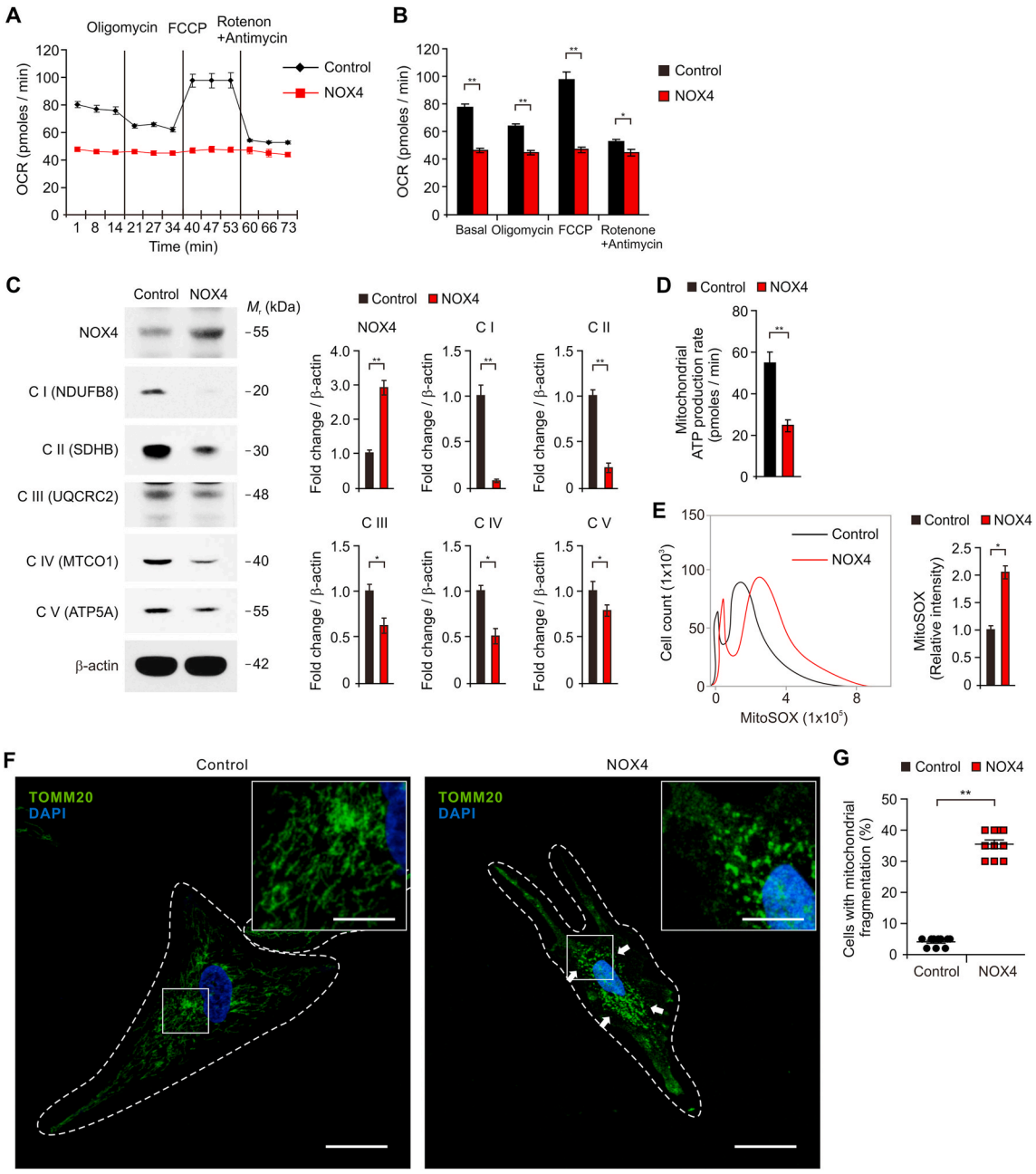

Fig. 5. The elevation of NOX4 promotes oxidative stress by impairment of mitochondrial metabolism via inhibition of mitochondrial respiration and ATP production in human astrocytes.

(A) The levels of oxygen consumption rate (OCR) as the parameter of mitochondrial respiration activity and (B) quantification of OCR levels in control (Control) and NOX4 overexpressing (NOX4) human astrocytes. Data are representative of three independent experiments. Data are mean ± SEM. **p < 0.01; *p < 0.05 using two-tailed Student's t-test. (C) Representative immunoblot analysis for five mitochondrial ETC protein levels (left) including NDUFB8 for Complex I (C I (NDUFB8)), SDHB for Complex II (C II (SDHB)), UQCRC2 for Complex III (C III (UQCRC2)), MTCO1 for Complex IV (C IV (MTCO1)) and ATP5F1A for Complex V (C V (ATP5F1A)) in control (Control) and NOX4 overexpressing (NOX4) human astrocytes. Quantification for protein levels of C I (NDUFB8, C II (SDHB), C III (UQCRC2), C IV (MTCO1) and C V (ATP5F1A) (right) in control (Control) and NOX4 overexpressing (NOX4) human astrocytes. For immunoblots, β-actin was used as a loading control. Data are representatives of three independent experiments. Data are mean ± standard deviation (SD). **p < 0.01; *p < 0.05 using two-tailed Student's t-test. (D) Quantification of mitochondrial ATP production rate in control (Control) and NOX4 overexpressing (NOX4) human astrocytes. Data are mean ± SD. **p < 0.01 using two-tailed Student's t-test. (E) Quantification of mtROS levels using MitoSOX staining in control (Control) and NOX4 overexpressing (NOX4) human astrocytes. Data are mean ± SD. *p < 0.05 using two-tailed Student's t-test. (F) Representative immunofluorescence images of mitochondrial morphology for mitochondria fragmentation by Tomm20 staining in control (Control) and NOX4 overexpressing (NOX4) human astrocytes showing Tomm20 (green) (n = 10 per group). DAPI-stained nuclei are shown in blue. The fragmentation of mitochondria is indicated (white arrows). Scale bars, 20 μm. Magnified views of the selected regions (upper right); scale bars, 5 μm. (G) Quantification of cells with mitochondrial fragmentation from immunofluorescence images of mitochondrial morphology in control (Control) and NOX4 overexpressing (NOX4) human astrocytes (n = 10 per group). (The percent of morphological dead cells in a total of 100 cells of 10 individual images per group was calculated). Symbols expressed by white dotted line indicate the shape of cells. Data are mean ± SD. **, p < 0.01 by Student's two-tailed *t*-test. (For interpretation of the references to colour in this figure legend, the reader is referred to the Web version of this article.)

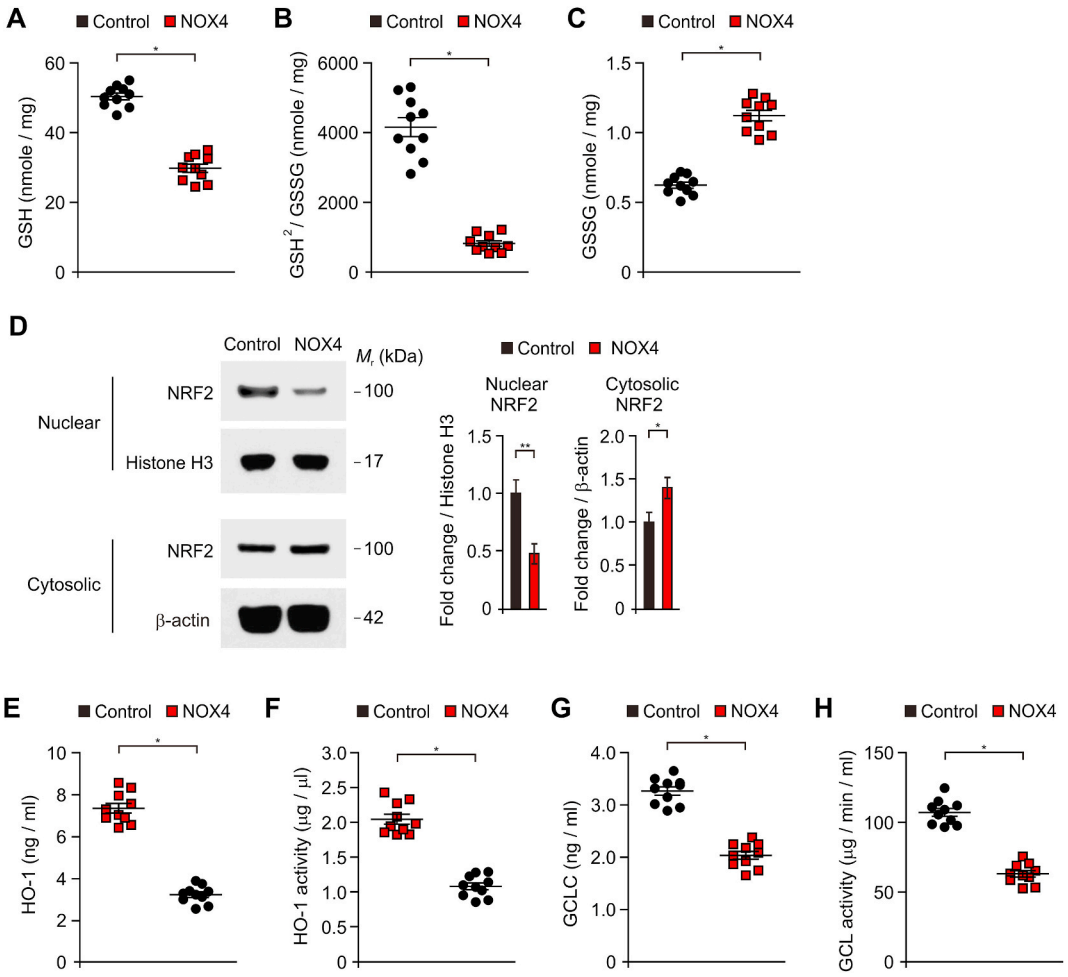

Fig. 6. NOX4-induced mitochondrial metabolic impairment induces oxidative stress by inhibition of cellular antioxidant process in human astrocytes. (A-C) Quantification of (A) reduced GSH levels, (B) ratio of GSH^2/GSSG, and (C) GSSG levels in control (Control) and NOX4 overexpressing (NOX4) human astrocytes (n = 10 per group). Data are mean ± SD. *, $p < 0.01$ by Student's two-tailed *t*-test. (D) Representative immunoblot analysis for nuclear and cytosolic NRF2 in control (Control) and NOX4 overexpressing (NOX4) human astrocytes. For immunoblots, Histone H3 (nuclear) and β-actin (cytosolic) was used as a loading control. Data are representative of three independent experiments. Data are mean ± SD. **, $p < 0.01$; *, $p < 0.05$ using the two-tailed Student's t-test. (E–F) Quantification of (E) HO-1 protein levels, (F) HO-1 activity, (G) GCLC protein levels and (F) GCL activity in control (Control) and NOX4 overexpressing (NOX4) human astrocytes (n = 10 per group). Data are mean ± SD. *, $p < 0.01$ by Student's two-tailed *t*-test.

NOX4 in reactive astrocytes is needed.

The features of ferroptosis, such as iron dysregulation, lipid peroxidation and inflammation, are important pathological events of AD and cognitive dysfunction [52]. Since the brain contains the high levels of polyunsaturated fatty acids (PUFAs) in its membrane rich architecture, lipid peroxidation could be a major feature of ferroptosis in AD [53,54]. A previous study has shown that a product of lipid peroxidation is increased in brain of patients with AD [55]. As the driving force of ferroptosis, a high level of lipid peroxidation can disrupt cellular function [56]. The abundant diffusible products of lipid peroxidation are chemically reactive aldehydes including malondialdehyde (MDA), acrolein, 4-hydroxy-2-hexenal (4-HHE), and 4-hydroxy-2-nonenal (4-HNE) [57,58]. Reactive aldehydes from lipid peroxidation have biological active functions [59]. 4-HNE, an electrophilic lipid peroxidation product, also has various cytotoxic effects of lipid peroxidation such as depletion of glutathione, dysfunction of structural proteins, reduction in enzyme activities, and induction of cell death [60]. Based on hormetic effects of 4-HNE, low physiological levels of 4-HNE can provide positive effects on cell function including cell proliferation and signaling pathway such as tyrosine kinase receptor (TKR) activation and downstream kinase signaling [61–67]. High levels of 4-HNE found in pathological conditions or diseases which are associated with cellular stress and dysfunction, cellular damage and pro-apoptotic signaling [68–73]. In pathogenesis of neurodegenerative diseases, the high levels of 4-HNE are involved in oxidative stress of AD or Parkinson's diseases [70–73]. Consistent with previous studies, our results suggest that the elevation of 4-HNE levels induces impairment of astrocytes in patients with AD and human astrocytes. Although the role of lipid peroxidation has been discovered in cell dysfunction and death during neuronal degeneration [74,75], the upstream molecular target in the regulation of ferroptosis by lipid peroxidation in AD remains unclear. Our results suggest that NOX4 is an upstream molecular target of lipid peroxidation-derived ferroptosis in impaired astrocytes during AD. Our findings showed that the elevation of NOX4 promotes ferroptosis by the accumulation of 4-HNE and morphological cytotoxicity. Ferroptosis-derived dead cells can release damage-associated molecular patterns (DAMPs) and lipid metabolites that can cause an elevation of inflammation [76,77]. Since the secreted molecules by NOX4-induced ferroptosis might be selective diagnostic markers in patients with AD, further study is needed to identify secreted molecules by NOX4-induced ferroptosis in patient with AD.

The redox imbalance and oxidative stress are linked to neurodegeneration in AD [1–4]. The high production of ROS is associated with excessive intracellular lipid accumulation such as diacylglycerol (DAG)

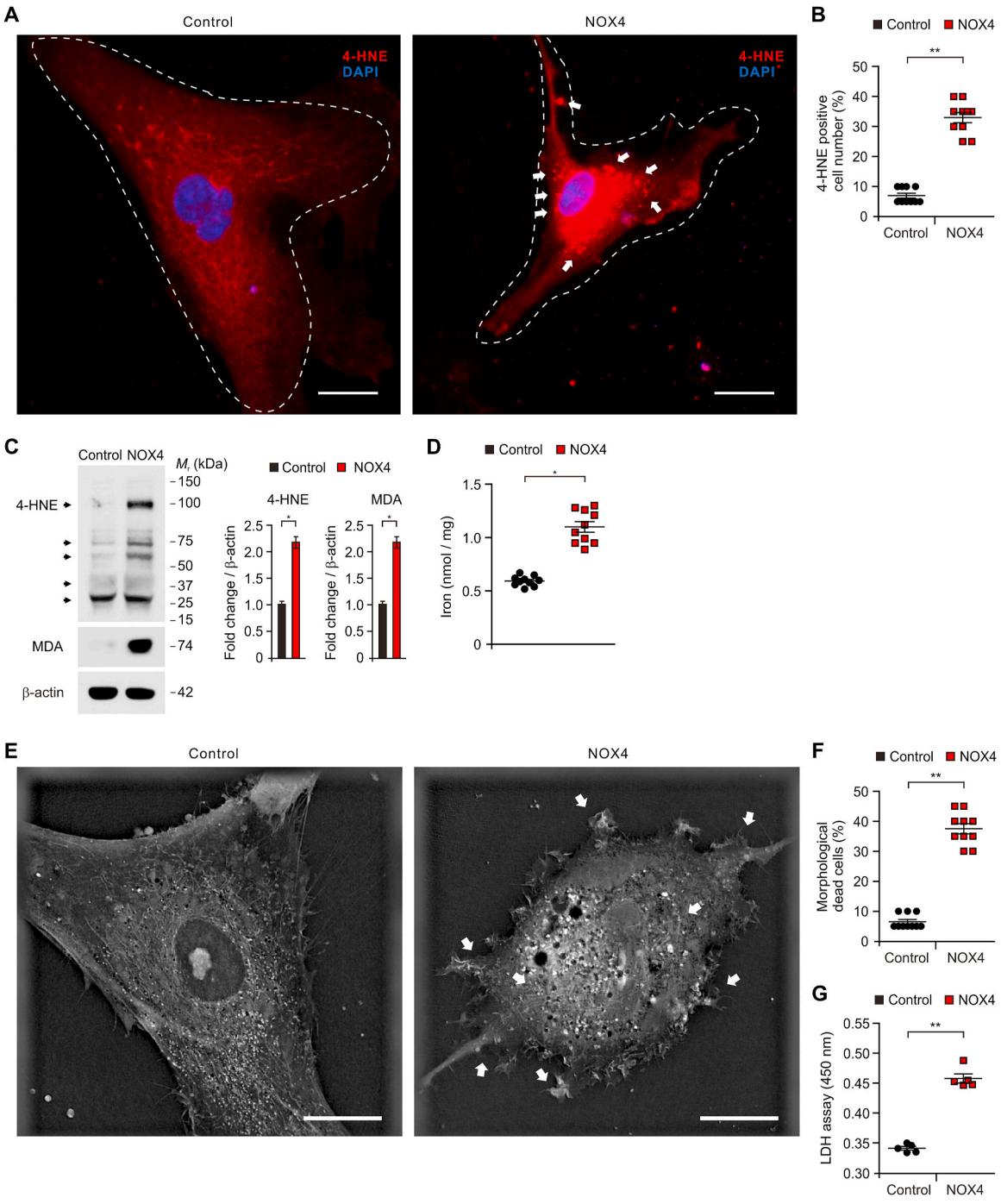

Fig. 7. NOX4 promotes ferroptosis by oxidative stress-induced lipid peroxidation in human astrocytes.
(A) Representative immunofluorescence images of 4-HNE expression in control (Control) and NOX4 overexpressing (NOX4) human astrocytes showing 4-HNE (red) (n = 10 per group). DAPI-stained nuclei are shown in blue. The shape of cells showed shrinkage and lipid peroxidation-derived droplets in the plasma membrane were indicated (white arrows). Symbols expressed by white dotted line indicate the shape of cells. Scale bars, 20 μm. (B) Quantification of 4-HNE positive astrocytes from immunofluorescence images in control (Control) and NOX4 overexpressing (NOX4) human astrocytes (n = 10 per group) (The percent of morphological dead cells in a total of 100 cells of 10 individual images per group was calculated). Data are mean ± standard deviation (SD). **, $p < 0.01$ by Student's two-tailed *t*-test. (C) Representative immunoblot analysis for 4-HNE and MDA protein levels (left) and quantification for 4-HNE and MDA protein levels in control (Control) and NOX4 overexpressing (NOX4) human astrocytes. For immunoblots, β-actin was used as a loading control. Data are representative of three independent experiments. Data are mean ± SD. *$p < 0.05$ using the two-tailed Student's t-test. (D) Quantification of iron levels in control (Control) and NOX4 overexpressing (NOX4) human astrocytes (n = 10 per group). Data are mean ± standard deviation (SD). *, $p < 0.05$ by Student's two-tailed *t*-test. (E) Representative 3D images of control (Control) and NOX4 overexpressing (NOX4) human astrocytes (n = 10 images per group). The morphological features of cytotoxicity were indicated (white arrows). Scale bars, 20 μm. (F) Quantification of the morphological dead cells in control (Control) and NOX4 overexpressing (NOX4) human astrocytes (n = 10 per group) (The percent of morphological dead cells in total 100 cells in 10 individual images per group). Data are mean ± SD. **, $p < 0.01$ using the two-tailed Student's t-test. (G) Cytotoxicity assay in control (Control) and NOX4 overexpressing (NOX4) human astrocytes was determined by lactate dehydrogenase (LDH) levels. Data are representatives of three independent experiments. Each experiment was done in triplicate. Data are mean ± SD. **, $p < 0.01$ using two-tailed Student's t-test. (For interpretation of the references to colour in this figure legend, the reader is referred to the Web version of this article.)

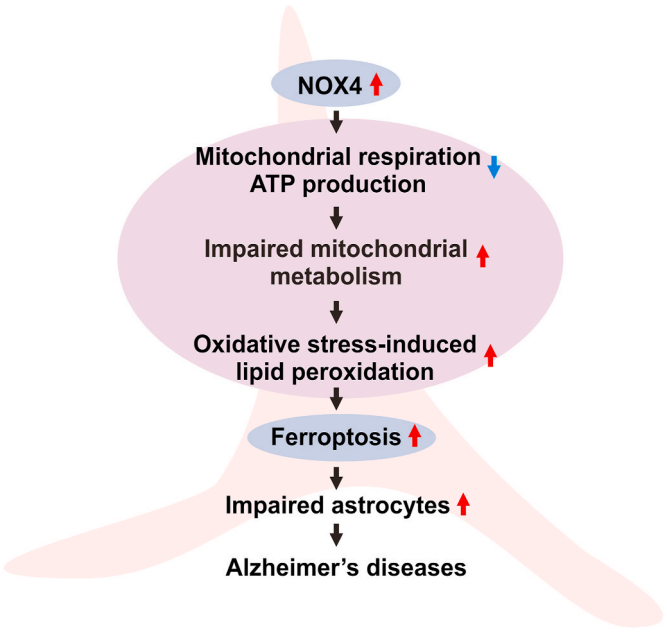

Fig. 8. A schematic diagram to summarize our new findings.
Red arrow means an increase. Blue arrow means a decrease in the diagram. (For interpretation of the references to colour in this figure legend, the reader is referred to the Web version of this article.)

and ceramide [78–80]. Since the high levels of ceramide contribute to formation of amyloid β-peptides [81–83], the accumulation of ceramide may have the effects of neurotoxicity in AD. Also, mitochondrial dysfunction including the excessive production of mtROS contributes to the induction of neuronal apoptosis [84–86]. Consistent with previous studies, our results suggest that NOX4-induced mitochondrial impairment and lipid peroxidation might be a critical pathway for neurodegeneration in AD related to redox imbalance and oxidative stress.

In summary, our study demonstrates that NOX4 promotes ferroptosis of astrocytes by oxidative stress-induced lipid peroxidation via impairment of mitochondrial metabolism as an important molecular mechanism in the impairment of astrocytes during AD.

Author contributions

M.W.P., I.D.Y. and J.-S.M. conceived the study. M.W.P. contributes to all experiments. M.W.P., H.W.C., J.K., J.H.K., and H.Y. performed analysis for IF images and 3D images. M.W.P., I.D.Y., S.Y. and N.B. performed cytotoxicity analysis. M.W.P. and H.W.C. performed immune blot analysis. S.S.Y., I.D.Y. and J.-S.M. participated in data acquisition and interpretation of results. M.W.P. and J.-S.M. wrote the paper. J.-S.M. supervised the entire project. All authors read, revised, and approved the final manuscript.

Declaration of competing interest

The authors declare that they have no known competing financial interests or personal relationships that could have appeared to influence the work reported in this paper.

Acknowledgements

This work was supported by the National Research Foundation of Korea (NRF) grant (NRF-2019M3E5D1A02069062 to I.D.Y., NRF-2018R1D1A3B07047960 to S.S.Y., NRF-2021R1C1C1007810 and NRF-2019M3E5D1A02069071 to J.-S.M.) and Soonchunhyang University Research Fund.

Appendix A. Supplementary data

Supplementary data to this article can be found online at https://doi.org/10.1016/j.redox.2021.101947.

References

[1] D.J. Selkoe, Alzheimer's disease: genes, proteins, and therapy, Physiol. Rev. 81 (2) (2001) 741–766, https://doi.org/10.1152/physrev.2001.81.2.741.
[2] D.A. Butterfield, B. Halliwell, Oxidative stress, dysfunctional glucose metabolism and Alzheimer disease, Nat. Rev. Neurosci. 20 (3) (2019) 148–160, https://doi.org/10.1038/s41583-019-0132-6.
[3] W.J. Huang, X. Zhang, W.W. Chen, Role of oxidative stress in Alzheimer's disease, Biomed Rep 4 (5) (2016) 519–522, https://doi.org/10.3892/br.2016.630.
[4] D.A. Butterfield, J. Drake, C. Pocernich, A. Castegna, Evidence of oxidative damage in Alzheimer's disease brain: central role for amyloid beta-peptide, Trends Mol. Med. 7 (12) (2001) 548–554, https://doi.org/10.1016/s1471-4914(01)02173-6.
[5] J.M. Perez Ortiz, R.H. Swerdlow, Mitochondrial dysfunction in Alzheimer's disease: role in pathogenesis and novel therapeutic opportunities, Br. J. Pharmacol. 176 (18) (2019) 3489–3507, https://doi.org/10.1111/bph.14585.
[6] H. Wood, Mitochondrial dysfunction manifests in the early stages of Alzheimer disease, Nat. Rev. Neurol. 16 (5) (2020) 242, https://doi.org/10.1038/s41582-020-0353-3.
[7] X. Wang, W. Wang, L. Li, G. Perry, H.G. Lee, X. Zhu, Oxidative stress and mitochondrial dysfunction in Alzheimer's disease, Biochim. Biophys. Acta 1842 (8) (2014) 1240–1247, https://doi.org/10.1016/j.bbadis.2013.10.015.
[8] D.L. Marcus, C. Thomas, C. Rodriguez, K. Simberkoff, J.S. Tsai, J.A. Strafaci, M. L. Freedman, Increased peroxidation and reduced antioxidant enzyme activity in Alzheimer's disease, Exp. Neurol. 150 (1) (1998) 40–44, https://doi.org/10.1006/exnr.1997.6750.
[9] W.R. Markesbery, Oxidative stress hypothesis in Alzheimer's disease, Free Radic. Biol. Med. 23 (1) (1997) 134–147, https://doi.org/10.1016/s0891-5849(96)00629-6.
[10] J.N. Peoples, A. Saraf, N. Ghazal, T.T. Pham, J.Q. Kwong, Mitochondrial dysfunction and oxidative stress in heart disease, Exp. Mol. Med. 51 (12) (2019) 1–13, https://doi.org/10.1038/s12276-019-0355-7.
[11] M. Golpich, E. Amini, Z. Mohamed, R. Azman Ali, N. Mohamed Ibrahim, A. Ahmadiani, Mitochondrial dysfunction and biogenesis in neurodegenerative diseases: pathogenesis and treatment, CNS Neurosci. Ther. 23 (1) (2017) 5–22, https://doi.org/10.1111/cns.12655.
[12] M.T. Lin, M.F. Beal, Mitochondrial dysfunction and oxidative stress in neurodegenerative diseases, Nature 443 (7113) (2006) 787–795, https://doi.org/10.1038/nature05292.
[13] A. Rossi, G. Rigotto, G. Valente, V. Giorgio, E. Basso, R. Filadi, P. Pizzo, Defective mitochondrial Pyruvate flux affects cell bioenergetics in Alzheimer's disease-related models, Cell Rep. 30 (7) (2020) 2332–2348, https://doi.org/10.1016/j.celrep.2020.01.060, e10.
[14] G. Ricci, L. Volpi, L. Pasquali, L. Petrozzi, G. Siciliano, Astrocyte-neuron interactions in neurological disorders, J. Biol. Phys. 35 (4) (2009) 317–336, https://doi.org/10.1007/s10867-009-9157-9.
[15] A. Rocchi, D. Valensin, C. Aldinucci, G. Giani, R. Barbucci, E. Gaggelli, H. Kozlowski, G. Valensin, NMR metabolomic investigation of astrocytes interacted with $A\beta_{42}$ or its complexes with either copper(II) or zinc(II), J. Inorg. Biochem. 117 (2012) 326–333, https://doi.org/10.1016/j.jinorgbio.2012.08.021.
[16] C.R. Figley, P.W. Stroman, The role(s) of astrocytes and astrocyte activity in neurometabolism, neurovascular coupling, and the production of functional neuroimaging signals, Eur. J. Neurosci. 33 (4) (2011) 577–588, https://doi.org/10.1111/j.1460-9568.2010.07584.x.
[17] T. Ishibashi, K.A. Dakin, B. Stevens, P.R. Lee, S.V. Kozlov, C.L. Stewart, R.D. Fields, Astrocytes promote myelination in response to electrical impulses, Neuron 49 (6) (2006) 823–832, https://doi.org/10.1016/j.neuron.2006.02.006.
[18] R. Parri, V. Crunelli, An astrocyte bridge from synapse to blood flow, Nat. Neurosci. 6 (1) (2003) 5–6, https://doi.org/10.1038/nn0103-5.
[19] O. Pascual, K.B. Casper, C. Kubera, J. Zhang, R. Revilla-Sanchez, J.Y. Sul, H. Takano, S.J. Moss, K. McCarthy, P.G. Haydon, Astrocytic purinergic signaling coordinates synaptic networks, Science 310 (5745) (2005) 113–116, https://doi.org/10.1126/science.1116916.
[20] W. Walz, Role of astrocytes in the clearance of excess extracellular potassium, Neurochem. Int. 36 (4–5) (2000) 291–300, https://doi.org/10.1016/s0197-0186(99)00137-0.
[21] H. Phatnani, T. Maniatis, Astrocytes in neurodegenerative disease, Cold Spring Harb Perspect Biol 7 (6) (2015), https://doi.org/10.1101/cshperspect.a020628.
[22] V. Karkkainen, J. Magga, J. Koistinaho, T. Malm, Brain environment and Alzheimer's disease mutations affect the survival, migration and differentiation of neural progenitor cells, Curr. Alzheimer Res. 9 (9) (2012) 1030–1042, https://doi.org/10.2174/156720512803569028.
[23] I.D. Yoo, M.W. Park, H.W. Cha, S. Yoon, N. Boonpraman, S.S. Yi, J.S. Moon, Elevated CLOCK and BMAL1 contribute to the impairment of aerobic glycolysis from astrocytes in Alzheimer's disease, Int. J. Mol. Sci. 21 (21) (2020), https://doi.org/10.3390/ijms21217862.
[24] J. Rose, C. Brian, A. Pappa, M.I. Panayiotidis, R. Franco, Mitochondrial metabolism in astrocytes regulates brain bioenergetics, neurotransmission and redox balance, Front. Neurosci. 14 (2020) 536682, https://doi.org/10.3389/fnins.2020.536682.

[25] D. Nolfi-Donegan, A. Braganza, S. Shiva, Mitochondrial electron transport chain: oxidative phosphorylation, oxidant production, and methods of measurement, Redox Biol 37 (2020) 101674, https://doi.org/10.1016/j.redox.2020.101674.
[26] C. Vicente-Gutierrez, N. Bonora, V. Bobo-Jimenez, D. Jimenez-Blasco, I. Lopez-Fabuel, E. Fernandez, C. Josephine, G. Bonvento, J.A. Enriquez, A. Almeida, J. P. Bolaños, Astrocytic mitochondrial ROS modulate brain metabolism and mouse behaviour, Nat Metab 1 (2) (2019) 201–211, https://doi.org/10.1038/s42255-018-0031-6.
[27] J.G. Jackson, M.B. Robinson, Regulation of mitochondrial dynamics in astrocytes: mechanisms, consequences, and unknowns, Glia 66 (6) (2018) 1213–1234, https://doi.org/10.1002/glia.23252.
[28] C. Fiebig, S. Keiner, B. Ebert, I. Schäffner, R. Jagasia, D.C. Lie, R. Beckervordersandforth, Mitochondrial dysfunction in astrocytes impairs the generation of reactive astrocytes and enhances neuronal cell death in the cortex upon photothrombotic lesion, Front. Mol. Neurosci. 12 (2019) 40, https://doi.org/10.3389/fnmol.2019.00040.
[29] R. Guo, S. Zong, M. Wu, J. Gu, M. Yang, Architecture of human mitochondrial respiratory megacomplex I(2)III(2)IV(2), Cell 170 (6) (2017) 1247–1257, https://doi.org/10.1016/j.cell.2017.07.050, e12.
[30] R.Z. Zhao, S. Jiang, L. Zhang, Z.B. Yu, Mitochondrial electron transport chain, ROS generation and uncoupling (Review), Int. J. Mol. Med. 44 (1) (2019) 3–15, https://doi.org/10.3892/ijmm.2019.4188.
[31] S. Nemoto, K. Takeda, Z.X. Yu, V.J. Ferrans, T. Finkel, Role for mitochondrial oxidants as regulators of cellular metabolism, Mol. Cell Biol. 20 (19) (2000) 7311–7318, https://doi.org/10.1128/mcb.20.19.7311-7318.2000.
[32] B.R. Stockwell, J.P. Friedmann Angeli, H. Bayir, A.I. Bush, M. Conrad, S.J. Dixon, S. Fulda, S. Gascón, S.K. Hatzios, V.E. Kagan, K. Noel, X. Jiang, A. Linkermann, M. E. Murphy, M. Overholtzer, A. Oyagi, G.C. Pagnussat, J. Park, Q. Ran, C. S. Rosenfeld, K. Salnikow, D. Tang, F.M. Torti, S.V. Torti, S. Toyokuni, K. A. Woerpel, D.D. Zhang, Ferroptosis: a regulated cell death Nexus linking metabolism, Redox Biol. Dis. Cell 171 (2) (2017) 273–285, https://doi.org/10.1016/j.cell.2017.09.021.
[33] B.R. Stockwell, X. Jiang, The chemistry and biology of ferroptosis, Cell Chem Biol 27 (4) (2020) 365–375, https://doi.org/10.1016/j.chembiol.2020.03.013.
[34] M. Conrad, V.E. Kagan, H. Bayir, G.C. Pagnussat, B. Head, M.G. Traber, B. R. Stockwell, Regulation of lipid peroxidation and ferroptosis in diverse species, Genes Dev. 32 (9–10) (2018) 602–619, https://doi.org/10.1101/gad.314674.118.
[35] K. Bedard, K.H. Krause, The NOX family of ROS-generating NADPH oxidases: physiology and pathophysiology, Physiol. Rev. 87 (1) (2007) 245–313, https://doi.org/10.1152/physrev.00044.2005.
[36] Z. Nayernia, V. Jaquet, K.H. Krause, New insights on NOX enzymes in the central nervous system, Antioxidants Redox Signal. 20 (17) (2014) 2815–2837, https://doi.org/10.1089/ars.2013.5703.
[37] L. Serrander, L. Cartier, K. Bedard, B. Banfi, B. Lardy, O. Plastre, A. Sienkiewicz, L. Fórró, W. Schlegel, K.H. Krause, NOX4 activity is determined by mRNA levels and reveals a unique pattern of ROS generation, Biochem. J. 406 (1) (2007) 105–114, https://doi.org/10.1042/bj20061903.
[38] K. Ishii, H. Kitagaki, M. Kono, E. Mori, Decreased medial temporal oxygen metabolism in Alzheimer's disease shown by PET, J. Nucl. Med. 37 (7) (1996) 1159–1165.
[39] H. Tohgi, H. Yonezawa, S. Takahashi, N. Sato, E. Kato, M. Kudo, K. Hatano, T. Sasaki, Cerebral blood flow and oxygen metabolism in senile dementia of Alzheimer's type and vascular dementia with deep white matter changes, Neuroradiology 40 (3) (1998) 131–137, https://doi.org/10.1007/s002340050553.
[40] I. Lajoie, S. Nugent, C. Debacker, K. Dyson, F.B. Tancredi, A. Badhwar, S. Belleville, Y. Deschaintre, P. Bellec, J. Doyon, C. Bocti, S. Gauthier, D. Arnold, M.J. Kergoat, H. Chertkow, O. Monchi, R.D. Hoge, Application of calibrated fMRI in Alzheimer's disease, Neuroimage Clin 15 (2017) 348–358, https://doi.org/10.1016/j.nicl.2017.05.009.
[41] W.S. Liang, E.M. Reiman, J. Valla, T. Dunckley, T.G. Beach, A. Grover, T. L. Niedzielko, L.E. Schneider, D. Mastroeni, R. Caselli, W. Kukull, J.C. Morris, C. M. Hulette, D. Schmechel, J. Rogers, D.A. Stephan, Alzheimer's disease is associated with reduced expression of energy metabolism genes in posterior cingulate neurons, Proc. Natl. Acad. Sci. U. S. A. 105 (11) (2008) 4441–4446, https://doi.org/10.1073/pnas.0709259105.
[42] A.I. Casas, E. Geuss, P.W.M. Kleikers, S. Mencl, A.M. Herrmann, I. Buendia, J. Egea, S.G. Meuth, M.G. Lopez, C. Kleinschnitz, H. Schmidt, NOX4-dependent neuronal autotoxicity and BBB breakdown explain the superior sensitivity of the brain to ischemic damage, Proc. Natl. Acad. Sci. U. S. A. 114 (46) (2017) 12315–12320, https://doi.org/10.1073/pnas.1705034114.
[43] M.W. Ma, J. Wang, K.M. Dhandapani, D.W. Brann, Deletion of NADPH oxidase 4 reduces severity of traumatic brain injury, Free Radic. Biol. Med. 117 (2018) 66–75, https://doi.org/10.1016/j.freeradbiomed.2018.01.031.
[44] C. Behl, J.B. Davis, R. Lesley, D. Schubert, Hydrogen peroxide mediates amyloid beta protein toxicity, Cell 77 (6) (1994) 817–827, https://doi.org/10.1016/0092-8674(94)90131-7.
[45] S. Miranda, C. Opazo, L.F. Larrondo, F.J. Muñoz, F. Ruiz, F. Leighton, N. C. Inestrosa, The role of oxidative stress in the toxicity induced by amyloid beta-peptide in Alzheimer's disease, Prog. Neurobiol. 62 (6) (2000) 633–648, https://doi.org/10.1016/s0301-0082(00)00015-0.
[46] A.Y. Abramov, L. Canevari, M.R. Duchen, Beta-amyloid peptides induce mitochondrial dysfunction and oxidative stress in astrocytes and death of neurons through activation of NADPH oxidase, J. Neurosci. 24 (2) (2004) 565–575, https://doi.org/10.1523/jneurosci.4042-03.2004.
[47] A.J. Bruce-Keller, S. Gupta, A.G. Knight, T.L. Beckett, J.M. McMullen, P.R. Davis, M.P. Murphy, L.J. Van Eldik, D. St Clair, J.N. Keller, Cognitive impairment in humanized APP×PS1 mice is linked to Aβ(1-42) and NOX activation, Neurobiol. Dis. 44 (3) (2011) 317–326, https://doi.org/10.1016/j.nbd.2011.07.012.
[48] R. Nortley, N. Korte, P. Izquierdo, C. Hirunpattarasilp, A. Mishra, Z. Jaunmuktane, V. Kyrargyri, T. Pfeiffer, L. Khennouf, C. Madry, H. Gong, A. Richard-Loendt, W. Huang, T. Saito, T.C. Saido, S. Brandner, H. Sethi, D. Attwell, Amyloid β oligomers constrict human capillaries in Alzheimer's disease via signaling to pericytes, Science 365 (6450) (2019), https://doi.org/10.1126/science.aav9518.
[49] U. Wilhelmsson, E.A. Bushong, D.L. Price, B.L. Smarr, V. Phung, M. Terada, M. H. Ellisman, M. Pekny, Redefining the concept of reactive astrocytes as cells that remain within their unique domains upon reaction to injury, Proc. Natl. Acad. Sci. U. S. A. 103 (46) (2006) 17513–17518, https://doi.org/10.1073/pnas.0602841103.
[50] B.G. Perez-Nievas, A. Serrano-Pozo, Deciphering the astrocyte reaction in Alzheimer's disease, Front. Aging Neurosci. 10 (2018) 114, https://doi.org/10.3389/fnagi.2018.00114.
[51] H. Chun, C.J. Lee, Reactive astrocytes in Alzheimer's disease: a double-edged sword, Neurosci. Res. 126 (2018) 44–52, https://doi.org/10.1016/j.neures.2017.11.012.
[52] W.S. Hambright, R.S. Fonseca, L. Chen, R. Na, Q. Ran, Ablation of ferroptosis regulator glutathione peroxidase 4 in forebrain neurons promotes cognitive impairment and neurodegeneration, Redox Biol 12 (2017) 8–17, https://doi.org/10.1016/j.redox.2017.01.021.
[53] J.T. Coyle, P. Puttfarcken, Oxidative stress, glutamate, and neurodegenerative disorders, Science 262 (5134) (1993) 689–695, https://doi.org/10.1126/science.7901908.
[54] D. Praticò, S. Sung, Lipid peroxidation and oxidative imbalance: early functional events in Alzheimer's disease, J Alzheimers Dis 6 (2) (2004) 171–175, https://doi.org/10.3233/jad-2004-6209.
[55] W.R. Markesbery, M.A. Lovell, Four-hydroxynonenal, a product of lipid peroxidation, is increased in the brain in Alzheimer's disease, Neurobiol. Aging 19 (1) (1998) 33–36, https://doi.org/10.1016/s0197-4580(98)00009-8.
[56] W.S. Yang, B.R. Stockwell, Ferroptosis: death by lipid peroxidation, Trends Cell Biol. 26 (3) (2016) 165–176, https://doi.org/10.1016/j.tcb.2015.10.014.
[57] C. Schneider, K.A. Tallman, N.A. Porter, A.R. Brash, Two distinct pathways of formation of 4-hydroxynonenal. Mechanisms of nonenzymatic transformation of the 9- and 13-hydroperoxides of linoleic acid to 4-hydroxyalkenals, J. Biol. Chem. 276 (24) (2001) 20831–20838, https://doi.org/10.1074/jbc.M101821200.
[58] N.A. Porter, S.E. Caldwell, K.A. Mills, Mechanisms of free radical oxidation of unsaturated lipids, Lipids 30 (4) (1995) 277–290, https://doi.org/10.1007/bf02536034.
[59] H. Esterbauer, R.J. Schaur, H. Zollner, Chemistry and biochemistry of 4-hydroxy-nonenal, malonaldehyde and related aldehydes, Free Radic. Biol. Med. 11 (1) (1991) 81–128, https://doi.org/10.1016/0891-5849(91)90192-6.
[60] J.E. Craighead, Pathology of Environmental and Occupational Disease, Mosby, 1995.
[61] S. Pizzimenti, S. Laurora, F. Briatore, C. Ferretti, M.U. Dianzani, G. Barrera, Synergistic effect of 4-hydroxynonenal and PPAR ligands in controlling human leukemic cell growth and differentiation, Free Radic. Biol. Med. 32 (3) (2002) 233–245, https://doi.org/10.1016/s0891-5849(01)00798-5.
[62] T. Ishii, K. Itoh, E. Ruiz, D.S. Leake, H. Unoki, M. Yamamoto, G.E. Mann, Role of Nrf2 in the regulation of CD36 and stress protein expression in murine macrophages: activation by oxidatively modified LDL and 4-hydroxynonenal, Circ. Res. 94 (5) (2004) 609–616, https://doi.org/10.1161/01.RES.0000119171.44657.45.
[63] H. Minekura, T. Kumagai, Y. Kawamoto, F. Nara, K. Uchida, 4-Hydroxy-2-nonenal is a powerful endogenous inhibitor of endothelial response, Biochem. Biophys. Res. Commun. 282 (2) (2001) 557–561, https://doi.org/10.1006/bbrc.2001.4586.
[64] G. Brunetti, G. Di Rosa, M. Scuto, M. Leri, M. Stefani, C. Schmitz-Linneweber, V. Calabrese, N. Saul, Healthspan maintenance and prevention of Parkinson's-like phenotypes with hydroxytyrosol and oleuropein aglycone in C. elegans, Int. J. Mol. Sci. 21 (7) (2020), https://doi.org/10.3390/ijms21072588.
[65] V. Calabrese, A. Santoro, D. Monti, R. Crupi, R. Di Paola, S. Latteri, S. Cuzzocrea, M. Zappia, J. Giordano, E.J. Calabrese, C. Franceschi, Aging and Parkinson's Disease: inflammaging, neuroinflammation and biological remodeling as key factors in pathogenesis, Free Radic. Biol. Med. 115 (2018) 80–91, https://doi.org/10.1016/j.freeradbiomed.2017.10.379.
[66] V. Calabrese, C. Cornelius, A.T. Dinkova-Kostova, E.J. Calabrese, M.P. Mattson, Cellular stress responses, the hormesis paradigm, and vitagenes: novel targets for therapeutic intervention in neurodegenerative disorders, Antioxidants Redox Signal. 13 (11) (2010) 1763–1811, https://doi.org/10.1089/ars.2009.3074.
[67] R. Fusco, M. Cordaro, T. Genovese, D. Impellizzeri, R. Siracusa, E. Gugliandolo, A. F. Peritore, R. D'Amico, R. Crupi, S. Cuzzocrea, R. Di Paola, Adelmidrol: a new promising antioxidant and anti-inflammatory therapeutic tool in pulmonary fibrosis, Antioxidants (Basel) 9 (7) (2020), https://doi.org/10.3390/antiox9070601.
[68] K.J. Barnham, C.L. Masters, A.I. Bush, Neurodegenerative diseases and oxidative stress, Nat. Rev. Drug Discov. 3 (3) (2004) 205–214, https://doi.org/10.1038/nrd1330.
[69] K. Jomova, D. Vondrakova, M. Lawson, M. Valko, Metals, oxidative stress and neurodegenerative disorders, Mol. Cell. Biochem. 345 (1–2) (2010) 91–104, https://doi.org/10.1007/s11010-010-0563-x.
[70] S.S. Hardas, R. Sultana, A.M. Clark, T.L. Beckett, L.I. Szweda, M.P. Murphy, D. A. Butterfield, Oxidative modification of lipoic acid by HNE in Alzheimer disease brain, Redox Biol 1 (2013) 80–85, https://doi.org/10.1016/j.redox.2013.01.002.
[71] A. Takeda, M.A. Smith, J. Avila, A. Nunomura, S.L. Siedlak, X. Zhu, G. Perry, L. M. Sayre, In Alzheimer's disease, heme oxygenase is coincident with Alz50, an

epitope of tau induced by 4-hydroxy-2-nonenal modification, J. Neurochem. 75 (3) (2000) 1234–1241, https://doi.org/10.1046/j.1471-4159.2000.0751234.x.
[72] X. Zhu, R.J. Castellani, P.I. Moreira, G. Aliev, J.C. Shenk, S.L. Siedlak, P.L.R. Harris, H. Fujioka, L.M. Sayre, P.A. Szweda, L.I. Szweda, M.A. Smith, G. Perry, Hydroxynonenal-generated crosslinking fluorophore accumulation in Alzheimer disease reveals a dichotomy of protein turnover, Free Radic. Biol. Med. 52 (3) (2012) 699–704, https://doi.org/10.1016/j.freeradbiomed.2011.11.004.
[73] A. Yoritaka, N. Hattori, K. Uchida, M. Tanaka, E.R. Stadtman, Y. Mizuno, Immunohistochemical detection of 4-hydroxynonenal protein adducts in Parkinson disease, Proc. Natl. Acad. Sci. U. S. A. 93 (7) (1996) 2696–2701, https://doi.org/10.1073/pnas.93.7.2696.
[74] M.P. Mattson, Modification of ion homeostasis by lipid peroxidation: roles in neuronal degeneration and adaptive plasticity, Trends Neurosci. 21 (2) (1998) 53–57, https://doi.org/10.1016/s0166-2236(97)01188-0.
[75] J.N. Keller, M.P. Mattson, Roles of lipid peroxidation in modulation of cellular signaling pathways, cell dysfunction, and death in the nervous system, Rev. Neurosci. 9 (2) (1998) 105–116, https://doi.org/10.1515/revneuro.1998.9.2.105.
[76] A. Linkermann, R. Skouta, N. Himmerkus, S.R. Mulay, C. Dewitz, F. De Zen, A. Prokai, G. Zuchtriegel, F. Krombach, P.S. Welz, R. Weinlich, T. Vanden Berghe, P. Vandenabeele, M. Pasparakis, M. Bleich, J.M. Weinberg, C.A. Reichel, J. H. Bräsen, U. Kunzendorf, H.J. Anders, B.R. Stockwell, D.R. Green, S. Krautwald, Synchronized renal tubular cell death involves ferroptosis, Proc. Natl. Acad. Sci. U. S. A. 111 (47) (2014) 16836–16841, https://doi.org/10.1073/pnas.1415518111.
[77] J.P. Friedmann Angeli, M. Schneider, B. Proneth, Y.Y. Tyurina, V.A. Tyurin, V. J. Hammond, N. Herbach, M. Aichler, A. Walch, E. Eggenhofer, D. Basavarajappa, O. Rådmark, S. Kobayashi, T. Seibt, H. Beck, F. Neff, I. Esposito, R. Wanke, H. Förster, O. Yefremova, M. Heinrichmeyer, G.W. Bornkamm, E.K. Geissler, S. B. Thomas, B.R. Stockwell, V.B. O'Donnell, V.E. Kagan, J.A. Schick, M. Conrad, Inactivation of the ferroptosis regulator Gpx4 triggers acute renal failure in mice, Nat. Cell Biol. 16 (12) (2014) 1180–1191, https://doi.org/10.1038/ncb3064.
[78] S.M. de la Monte, M. Tong, J.R. Wands, The 20-year Voyage aboard the Journal of Alzheimer's disease: docking at 'type 3 diabetes', environmental/exposure factors, pathogenic mechanisms, and potential treatments, J Alzheimers Dis 62 (3) (2018) 1381–1390, https://doi.org/10.3233/jad-170829.
[79] M. Jazvinšćak Jembrek, P.R. Hof, G. Šimić, Ceramides in Alzheimer's disease: key mediators of neuronal apoptosis induced by oxidative stress and Aβ accumulation, Oxid Med Cell Longev (2015) 346783, https://doi.org/10.1155/2015/346783.
[80] S.M. de la Monte, Brain insulin resistance and deficiency as therapeutic targets in Alzheimer's disease, Curr. Alzheimer Res. 9 (1) (2012) 35–66, https://doi.org/10.2174/156720512799015037.
[81] M. Tong, S.M. de la Monte, Mechanisms of ceramide-mediated neurodegeneration, J Alzheimers Dis 16 (4) (2009) 705–714, https://doi.org/10.3233/jad-2009-0983.
[82] W. Ahmad, B. Ijaz, K. Shabbiri, F. Ahmed, S. Rehman, Oxidative toxicity in diabetes and Alzheimer's disease: mechanisms behind ROS/RNS generation, J. Biomed. Sci. 24 (1) (2017) 76, https://doi.org/10.1186/s12929-017-0379-z.
[83] L. Ho, W. Qin, P.N. Pompl, Z. Xiang, J. Wang, Z. Zhao, Y. Peng, G. Cambareri, A. Rocher, C.V. Mobbs, P.R. Hof, G.M. Pasinetti, Diet-induced insulin resistance promotes amyloidosis in a transgenic mouse model of Alzheimer's disease, Faseb. J. 18 (7) (2004) 902–904, https://doi.org/10.1096/fj.03-0978fje.
[84] H. Zhou, X. Liu, L. Liu, Z. Yang, S. Zhang, M. Tang, Y. Tang, Q. Dong, R. Hu, Oxidative stress and apoptosis of human brain microvascular endothelial cells induced by free fatty acids, J. Int. Med. Res. 37 (6) (2009) 1897–1903, https://doi.org/10.1177/147323000903700627.
[85] B. Diaz, L. Fuentes-Mera, A. Tovar, T. Montiel, L. Massieu, H.G. Martínez-Rodríguez, A. Camacho, Saturated lipids decrease mitofusin 2 leading to endoplasmic reticulum stress activation and insulin resistance in hypothalamic cells, Brain Res. 1627 (2015) 80–89, https://doi.org/10.1016/j.brainres.2015.09.014.
[86] M. Maciejczyk, E. Żebrowska, A. Chabowski, Insulin resistance and oxidative stress in the brain: what's new? Int. J. Mol. Sci. 20 (4) (2019) https://doi.org/10.3390/ijms20040874.